Chapter III

A Variational Assimilation Method for Satellite and Conventional Data: A Revised Basic Model IIB

Gary L. Achtemeier, Robert W. Scott, and J. Chen
Office of Climate and Meteorology
Division of Atmospheric Sciences
Illinois State Water Survey
Champaign, Illinois 61820

ABSTRACT

A variational objective analysis technique that modifies observations of temperature, height, and wind on the cyclone scale to satisfy the five "primitive" model forecast equations is presented. This analysis method overcomes all of the problems that hindered previous versions - problems such as over-determination, time consistency, solution method, and constraint decoupling. A preliminary evaluation of the method shows that it converges rapidly, the divergent part of the wind is strongly coupled in the solution, fields of height and temperature are well-preserved, and derivative quantities such as vorticity and divergence are improved. Problem areas are systematic increases in the horizontal velocity components, and large magnitudes of the local tendencies of the horizontal velocity components. The preliminary evaluation makes note of these problems but detailed evaluations required to determine the origin of these problems await future research.

1. Introduction

This study was designed to determine the feasibility of a constrained objective analysis based upon the variational methodology of Sasaki (1958, 1970). The method uses as dynamic constraints the five primitive equations for a dry, adiabatic, and non-viscous atmosphere: the two nonlinear horizontal momentum equations, the continuity equation, the hydrostatic equation and the thermodynamic equation. The method is diagnostic, however

given the similarities between the dynamic constraints and the hydrodynamical equations of numerical prediction models, there exists a potential for extension of the technique to the derivation of initial fields for numerical models.

The potential of the variational methods for multivariate objective analyses has been explored with many dynamic constraints. Some of the studies and the constraints used are: the geostrophic approximation (Sasaki, 1958), the continuity equation (O,Brien, 1970; Dickerson, 1978; Sherman, 1978; Ray et al., 1978), divergence and vorticity (Schaefer and Doswell, 1979), the balance equation (Stephens, 1970), the two horizontal momentum equations (Lewis and Grason, 1972; Bloom, 1983), the two horizontal momentum and hydrostatic equation (Lewis, 1972), and the two horizontal momentum, thermodynamic, and hydrostatic equations (Achtemeier, 1975).

Past attempts to develop a multivariate objective analysis based upon Sasaki's variational method with the five "primitive" equations as dynamical constraints have encountered several fundamental problems. Courant (1936) showed that the number of subsidiary conditions (dynamic constraints) must be at least one less than the number of adjustable dependent variables else the problem is overdetermined and a solution is not guaranteed. The over-specification problem must be solved as the five primitive equations form a closed set with five dependent variables.

The Euler-Lagrange operations yield local tendencies of the Lagrange multipliers if the local tendencies of the temperature or

the horizontal velocity components are explicit in the dynamic constraints. Boundary conditions for these terms are unknown. The problem of time consistency in variational problems has been explored by Lewis (1980, 1982) and Lewis et al (1983). More recently, the time consistency problem has been found more tractable through use of the adjoint method (Lewis and Derber, 1985; Talagrand and Courtier, 1987).

Achtemeier (1975) found that the Euler-Lagrange equations decoupled the divergent part of the wind from the remainder of the adjustment with the result that the continuity equation was not satisfied. Attempts to constrain the local tendencies of velocity and temperature to require exact solution of the continuity equation did not solve the coupling problem (Achtemeier, 1979).

The methodology to circumvent the above problems and the theoretical development of a primitive equation variational objective analysis is presented in the next section (mathematical details are presented in Appendices A, B,and C.) The method is evaluated in Section 3.

2. Theoretical Development

The objective analysis is designed for a terrain-following coordinate surface. We used a nonlinear vertical coordinate created from two functions that are piecewise continuous through the second derivatives. In this coordinate system, all coordinate surfaces above a reference pressure level are pressure surfaces.

The dynamical equations appear in their simplest form in pressure coordinates. Furthermore, hydrostatic truncation errors are confined to coordinate surfaces below the reference pressure level. The problems of reducing hydrostatic truncation error along terrain-following coordinate surfaces has been the subject of considerable investigation (Kurihara, 1968; Gary 1973; Sundqvist, 1975, 1976; Janjic, 1977, 1989, and Achtemeier, 1990). The vertical coordinate is described in Appendix A.1.

Subjecting the pressure gradient terms of the horizontal momentum equations written in terrain-following coordinates to the variational operations separates the two pressure gradient terms and combines the large, now uncompensated terms with terms from the other equations. These uncompensated terrain terms can dominate the adjustment. A test found that these terms generated large error that caused the variational method to diverge.

The pressure gradient problem was solved by nondimensionalizing the dynamic constraints (Charney, 1948; Haltiner, 1971) and partitioning the hydrostatic terms to isolate the terrain part so that the variational adjustment could be performed on the meteorological partition. Appendix A.2 presents details of this procedure.

As regards the time consistency problem, Fjortoft (1952) found that the local change in the winds could be approximated by the translation of a weather system along an advective or steering current, usually a smoothed middle tropospheric wind. Therefore, the local tendencies of the velocity components were partitioned

into advective components, represented by the steady part of a weather system moving within a steering current, and developmental components, represented by the development of a weather system. Appendix A.3 describes the partition. The developmental components of u and v were defined as dependent variables to be subjected to the variational adjustment.

Appendix A.4 gives the five dynamic constraints as modified. Abridged forms of these equations are as follows:

$$M_1 = -v + \phi_x + DTU + HAU + VAU + EXT(M_1) = 0 \qquad (1)$$

$$M_2 = u + \phi_y + DTV + HAV + VAV + EXT(M_2) = 0 \qquad (2)$$

$$M_3 = Q(u_x + v_y)\Delta\sigma + (\dot{\sigma} - \dot{\sigma}_o) + EXT(M_3) = 0 \qquad (3)$$

$$M_4 = -\phi_\sigma + \gamma T + EXT(M_4) = 0 \qquad (4)$$

$$M_5 = LTT + HAT + VAT + VVT + \dot{\sigma}\sigma_\sigma + EXT(M_5) = 0 \qquad (5)$$

Conventional symbols are used. Abridged terms are defined as follows:

DTU(V) = developmental component of local tendency of u or v.

LTT = local tendency of T.

HAU(V or T) = horizontal advection of u (v or T) relative to a moving weather system.

VAU(V or T) = vertical advection of u (v or T).

VVT = product of vertical velocity with perturbations of stability.

$EXT(M_i)$ = extra terms that arise from any of the following sources:

a) Lambert conformal map image projection,

b) conversion into the nonlinear vertical coordinate,

c) expansion of the Coriolis and/or map scale factors.

Q = a normalized pressure thickness weight that arises from (b) above. For pressure levels above 700 mb, Q = 1.

The fourth term on the right hand side of (5) is the product of the layer average static stability with the vertical velocity.

These equations have been nondimensionalized and terms expressed in powers of the Rossby number. All terms identified by three letters (eg., LTU or EXT) are higher order terms - either multiplied by the Rossby number or of order 0.1 or terms that involve unadjusted (observed) variables.

Dependent variables are u, v, Φ, σ, T, ϵ_u, and ϵ_v. The latter two variables are the developmental components of the local tendencies of u and v. This formulation leaves five constraints and seven variables to be adjusted.

Following Achtemeier (1975), a variational objective analysis was developed for adjustments of the seven dependent variables subject to exact satisfaction of the dynamic constraints (1)-(5). As expected, the addition of the two new dependent variables (the developmental components of u and v) was sufficient to overcome the over-specification problem. As regards the time consistency problem, recomposition of the local tendencies of u and v from the advective and developmental components yielded tendencies that

compared favorably with observed 3-h changes in u and v. However, the decoupling problem remained. Attempts to readjust the divergent part of the wind by requiring the adjusted horizontal velocity components to satisfy the continuity equation through a "variational adjustment within a variational adjustment" were unsuccessful in satisfying all five constraints.

An analysis of the growth of the divergent part of the adjusted wind was performed to determine how the variational solution decoupled from the continuity equation. It was found that the divergent part of the wind is determined by adjustments through the higher order terms (HOT) of (1) and (2). The divergent components can be made to satisfy the continuity constraint if these higher order terms are made to satisfy a particular solution of the vorticity theorem. Define

$$F_5 = HOT(M_1) \tag{6}$$

$$F_6 = HOT(M_2) \tag{7}$$

so that,

$$M_1 = -v + \phi_x + F_5 = 0 \tag{8}$$

$$M_2 = u + \phi_y + F_6 = 0 \tag{9}$$

Forming the divergence,

$$u_x+v_y+F_{6x}-F_{5y}=0 \tag{10}$$

The function that must integrate to zero is

$$\int (u_x+v_y)\, d\sigma-\int (F_{6x}-F_{5y})\, d\sigma=0 \tag{11}$$

for the vertical velocity to vanish at the top at the top of the domain. Therefore, (11) is a particular solution of the integrated vorticity theorem, the particular solution also requiring that the horizontal divergence integrate to zero, a requirement for satisfaction of the continuity equation.

It is necessary to build (11) into the dynamic constraints if the decoupling problem is to be eliminated from the variational objective analysis. Define F_5 and F_6 as dependent variables and revise the dynamic constraints as follows:

$$M_1=-F_5+DTU+HAU+VAU+EXT(M_1)=0 \tag{12}$$

$$M_2=F_6+DTV+HAV+VAV+EXT(M_2)=0 \tag{13}$$

$$M_3=Q(F_{6x}-F_{5y})\,\Delta\sigma+(\dot{\sigma}-\dot{\sigma}_o)+EXT(M_3)=0 \tag{14}$$

$$M_4=\phi_\sigma+\gamma T+EXT(M_4)=0 \tag{15}$$

$$M_4 = LTT + HAT + VAT + VVT + \dot{\sigma}\sigma_\sigma + EXT(M_5) = 0 \tag{16}$$

$$M_6 = -v + \phi_x + F_5 = 0 \tag{17}$$

$$M_7 = u + \phi_y + F_6 = 0 \tag{18}$$

The variational objective analysis is developed from these seven constraints. The nine adjustable variables include the original seven plus F_5 and F_6.

The dynamical constraints are written on centered differences on an Arakawa D-grid (Mesinger and Arakawa, 1976). The finite difference operators and finite averaging operators are defined following Anthes and Warner (1978). The conversion of the constraints from differential form into finite differences is given in Appendix B.

The gridded fields of meteorological data to be modified are meshed with the dynamical equations through Sasaki's (1970) variational operations. To simplify the derivations, the frictional terms in the horizontal momentum equations and the diabatic heating term in the thermodynamic equation were set to zero.

The finite difference analog of the adjustment functional is,

$$\tilde{F} = \Delta x \Delta y \sum_i \sum_j a_i b_j I_{i,j} \tag{19}$$

The integrand, $I_{i,j}$ is

$$
\begin{aligned}
I = & \pi_1 (u-u^o)^2 + \pi_1 (v-v^o)^2 + \pi_2 (\dot{\sigma}-\dot{\sigma}^o)^2 \\
& + \pi_3 (\phi-\phi^o)^2 + \pi_4 (T-T^o)^2 + \pi_5 (\phi_x-\phi_x^o)^2 \\
& + \pi_5 (\phi_y-\phi_y^o)^2 + \pi_6 (\phi_\sigma-\phi_\sigma^o)^2 + \pi_7 (\epsilon_u-\epsilon_u^o)^2 \\
& + \pi_7 (\epsilon_v-\epsilon_v^o)^2 + \pi_8 (\epsilon_T-\epsilon_T^o)^2 + \pi_9 (F_5-F_5^o)^2 \\
& + \pi_9 (F_6-F_6^o)^2 + 2\sum_{i-1}^{7} \lambda_i M_i
\end{aligned}
\tag{20}
$$

The weights, π_i, are Gauss' precision moduli (Whittaker and Robinson, 1926). The gridded initial variables (u^o, v^o, σ^o, Φ^o, T^o, $\epsilon_u{}^o$, $_v{}^o$, $F_5{}^o$, $F_6{}^o$) enter in a least squares formulation and receive π_i according to their relative accuracies. The strong constraints to be satisfied exactly are introduced through the Lagrangian multipliers, λ_i.

Objectively modified meteorological variables are determined by requiring the first variation on F to vanish. A necessary condition for the existence of a stationary set is that the functions are determined from the domain of admissible functions as solutions of the Euler-Lagrange equations. The variation is to be carried out at every point (r,s) within the grid. Thus, upon setting the weights $a_i = b_j = 1$ and differentiating the integrand (20) with respect to the arbitrary variable $\alpha_{r,s}$, the Euler-Lagrange operator in finite differences is

The Euler-Lagrange equations resulting from the operations

$$\frac{\partial I_{i,j}}{\partial \alpha_{r,s}} = I_{\alpha_{i,j}} \frac{\partial \alpha_{i,j}}{\partial \alpha_{r,s}} = I_{\alpha_{i,j}} \delta^{i}_{r} \delta^{j}_{s} = 0 \tag{21}$$

specified by (21) are given in Appendix C [(C.7)-(C.16)]. Including the seven dynamic constraints, these complete a closed set of 17 of linear and nonlinear partial differential and algebraic equations. Solutions are difficult to obtain by conventional methods. Achtemeier (1975) proposed a cyclical solution method that moves higher order terms and terms involving unadjusted (observed) variables into forcing functions. These forcing functions may be expressed with observed variables at the first cycle and with previously adjusted variables at higher cycles. Therefore the forcing functions are known at each cycle. This method of solution is valid for the latitudes and scales of motion for which the Rossby number is less than one.

Use of the cyclical solution method yields the following set of linear Euler-Lagrange equations:

$$M_3 = -q_5 (F_{6x} - F_{5y}) \Delta\sigma + (\dot{\sigma} - \dot{\sigma}_o) + q_5 F_7 \Delta\sigma = 0 \tag{22}$$

$$M_4 = \phi_\sigma + \gamma T + \beta = 0 \tag{23}$$

$$M_6 = -v + \phi_x + F_5 = 0 \tag{24}$$

$$M_7 - u + \phi_y + F_6 = 0 \tag{25}$$

$$\overline{\pi}_5^{xy}\nabla^2\phi + \overline{\pi}_6^{\sigma}\phi_{\sigma\sigma} + \pi_{5x}\overline{\phi}_x^x + \pi_{5y}\overline{\phi}_y^y + \pi_{6\sigma}\overline{\phi}_{\sigma}^{\sigma} - \pi_3\phi + \lambda_{5x} + \lambda_{6y} + \lambda_{4\sigma} + F_4 = 0 \tag{26}$$

$$\pi_1 u + \lambda_6 + F_1 = 0 \tag{27}$$

$$\pi_1 v - \lambda_5 + F_2 = 0 \tag{28}$$

$$\pi_2\dot{\sigma} + \lambda_3 + F_3 = 0 \tag{29}$$

$$\pi_4 T + \gamma\lambda_4 + F_8 = 0 \tag{30}$$

$$\pi_7(\epsilon_u - \epsilon_u^o) + R_o\lambda_1 = 0 \tag{31}$$

$$\pi_7(\epsilon_v - \epsilon_v^o) + R_o\lambda_2 = 0 \tag{32}$$

$$\pi_8(\epsilon_T - \epsilon_T^o) + R_o\lambda_7 = 0 \tag{33}$$

$$\pi_9(F_5 - F_5^o) - \lambda_1 + \lambda_5 - \Delta\sigma(q_5\overline{\lambda}_3^{\sigma})_y = 0 \tag{34}$$

$$\pi_9(F_6 - F_6^o) - \lambda_2 + \lambda_6 + \Delta\sigma(q_5\overline{\lambda}_3^{\sigma})_x = 0 \tag{35}$$

As shown in Appendix C, variables may be easily eliminated among the equations. There results three diagnostic equations in geopotential, vorticity, and divergence,

$$\left(\overline{\pi}_5^{xy} + \pi_1\frac{\pi_{11}}{\pi_{10}}\right)\nabla^2\phi + \left(\overline{\pi}_6^{\sigma} + \frac{\pi_4}{\gamma^2}\right)\phi_{\sigma\sigma} + \pi_{5x}\overline{\phi}_x^x + \pi_{5y}\overline{\phi}_y^y + \left(\pi_{6\sigma} + \frac{\pi_4}{\gamma^2}\right)\overline{\phi}_{\sigma}^{\sigma} - \pi_3\phi = -G_4 - \frac{\pi_1}{\pi_{10}}(G_{2y} - G_{3x}) \tag{36}$$

$$\pi_{10}\zeta - \pi_{11}\nabla^2\phi = G_{2y} - G_{3x} \tag{37}$$

$$\nabla^2 [(\Delta\sigma)^2 q_5^2 \pi_2 D] - \pi_{10} D = \nabla^2 G_1 + G_{2x} + G_{3y} \tag{38}$$

Details regarding symbol definition are found in Appendix C.

The variational theory specifies natural boundary conditions that are consistent with the Euler-Lagrange equations. If it is assumed that there are no adjustments in the data along the boundaries, then the boundary conditions may be specified. In the latter case, the Lagrange multipliers, λ_i, are zero at the boundaries and the initial unadjusted values are used for the boundary conditions.

Initially, the Euler-Lagrange equations were solved with specified boundary conditions. These boundary conditions forced high frequency waves into the solutions for the velocity components near the boundaries. Divergences calculated from these velocity components gave large erroneous vertical velocities. We therefore returned to the natural boundary conditions.

The Euler-Lagrange operator for natural boundary conditions is,

$$\frac{\partial I}{\partial\left(\frac{\partial f_i}{\partial x_j}\right)} = 0 \tag{39}$$

Performing the operation specified by (39) produces a set of Euler-Lagrange boundary equations in Φ, u, v, and D. Details of the derivations are given in Appendix D. The boundary conditions for Φ are,

$$\begin{aligned}(\pi_5+\frac{\pi_1\pi_9}{\pi_1+\pi_9})\phi_x-\pi_5\phi_x^o-\frac{\pi_1\pi_9}{\pi_1+\pi_9}(u^o-F_5^o)=0\\(\pi_5+\frac{\pi_1\pi_9}{\pi_1+\pi_9})\phi_y-\pi_5\phi_y^o+\frac{\pi_1\pi_9}{\pi_1+\pi_9}(u^o+f_6^o)=0\end{aligned} \tag{40}$$

The boundary conditions for u and v that are consistent with (40) are,

$$\begin{aligned}(\pi_5+\pi_1\frac{\pi_5+\pi_9}{\pi_9})v-\pi_5(\phi_x^o-F_5^0)-\pi_1\frac{\pi_5+\pi_9}{\pi_9}v^o=0\\(\pi_5+\pi_1\frac{\pi_5+\pi_9}{\pi_9})u+\pi_5(\phi_y^o+F_6^o)-\pi_1\frac{\pi_5+\pi_9}{\pi_9}u^o=0\end{aligned} \tag{41}$$

The derivation of (40) placed a constraint upon the boundary conditions for the divergence, namely, that the divergence must be specified along two rows or columns at the boundaries.

Subject to the boundary conditions and specification of the precision moduli, (36)-(38) may be solved for the geopotential, vorticity and divergence. Coefficients for the second order partial derivative terms are always positive, the equations are elliptic, and thus solutions by standard methods are assured. Then u and v must be retrieved from the vorticity and the divergence.

A number of investigators (Sangster, 1960; Hawkins and Rosenthal, 1965; Shukla and Saha, 1974; Schaefer and Doswell, 1979;

Lynch, 1988) have proposed methods for reconstruction of the velocity components from the vorticity and divergence (or streamfunction and velocity potential). After investigating several of these methods, including those of Endlich (1967) and Bjilsma et al. (1986), it was determined that the Lynch method could be best adapted to the Arakawa D-grid with a minimum of error in reconstructing the velocity components.

First, the field of divergence was modified by a small constant so that Gauss' theorem,

$$\iint_A D\,da = \oint_s V_n\,ds \tag{42}$$

was satisfied. Then the u-component was reconstructed through

$$\nabla^2 u = D_x - \zeta_y \tag{43}$$

subject to mixed boundary conditions in u (obtained from (41)) along the y-boundaries and u_y obtained along the x-boundaries from

$$u_y = v_x - \zeta \tag{44}$$

Then, beginning at the lower x-boundary with v from (41),

$$v_y = D - u_x \tag{45}$$

was solved to find v uniquely.

3. Case Study Description and Preprocessing of Data

The data used to test the variational objective analysis consisted of rawinsonde temperature, height, and wind data at standard National Weather Service reporting sites shown in Fig. 1 for a large part of the United States and parts of southern Canada on 12 GMT 10 April 1979 and 00 GMT 11 April 1979. This case was originally selected because microwave temperature soundings coexisted with special 3-hr rawinsonde data over a large area of the central United States (small dashed-line box in Fig. 1) during a major cyclogenesis. The 3-hr rawinsonde data were used as ground truth for the local tendencies of the velocity components and temperature diagnosed from the variational objective analysis.

The data at 12 GMT 10 April 1979 described a weak, dissipating short wave moving northward over the Central Plains in advance of a more vigorous short wave. At 00 GMT 11 April, an intense jet streak moved northeastward over Oklahoma and Texas and triggered a mesoscale convective system over northern Texas that produced a number of fatalities at Wichita Falls, Texas.

The data were gridded from the observations by a modification of the Barnes (1964) objective technique that is designed to minimize analysis error at the boundaries of the field of data (Achtemeier, 1986) and to provide accurate derivatives within the

interior of the domain (Achtemeier, 1989). The analyses were done for 10 levels from 1000 mb to 100 mb. The horizontal grid was a 40x25 array with a 100 km grid spacing. Then thermodynamic data were converted to the nonlinear vertical coordinate through a hydrostatically consistent interpolation downward from the reference pressure level of 700 mb to the terrain-following coordinate surfaces. In addition, a smoothed version of the 600 mb wind velocity components was obtained through a single pass of the objective interpolation designed to reproduce the long wavelength features inherent in the data. The smoothed wind field served as the advective wind in the calculation of the advective part of the local tendencies of the velocity components.

The above analyses produced gridded fields of temperature, height, and u and v wind components. The initial fields of vertical velocity, developmental components of the local tendencies and F_5 and F_6 must be estimated from these data. Letting

$$\epsilon_T = -km\left(u\frac{\partial T}{\partial x}+v\frac{\partial T}{\partial y}\right) \tag{46}$$

the adiabatic vertical velocity can be found by solving (B.10) for σ. Then an adjusted vertical velocity can be found by a variational formulation using the continuity equation (Chance, 1986) that is similar to the O'Brien (1970) method with the exception that compatibility between the divergence and the vertical velocity is forced at each level. The relative weight accorded to the adiabatic vertical velocity is directly

proportional to the static stability. Thus the adiabatic vertical velocity receives the greater weight in areas of higher stability such as the stratosphere. This procedure keeps large erroneous vertical velocities generated by divergence error from being transferred from the troposphere into the stratosphere where,in product with the static stability terms of (B.10), would produce large errors in the adjusted time derivatives of temperature.

We have no way of estimating the developmental components of the velocity component tendencies from data collected at a single time. Therefore, these fields were set to zero. An alternative, if available, would be local tendencies from a numerical model.

The forcing function variables, F_5 and F_6 are estimated by substituting the initial variables into (B.4) and (B.6). Then F_5 and F_6 were adjusted to satisfy (11) with the exception that the integral of the divergence was replaced by the adjusted vertical velocity.

The resulting fields (and selected derivative fields) of T, Φ, u, v, σ, ϵ_u, ϵ_v, F_5, and F_6 were designated as unadjusted fields and entered into the variational objective analysis through the functional integrand, I, given by (20). The unadjusted quantities were accorded precision modulus weights according to the formula,

$$\pi_i = \frac{G_i(x,y)}{2\sigma_i^2} \qquad (47)$$

where the σ_i is the root-mean-square (RMS) error of observation for the ith variable. G_i is in general a function of observation density but G≡1 for this study. However, since observational errors are available only for u, v, Φ, and T, only π_1, π_3, and π_4 can be obtained from (47). the σ_i for the remaining unadjusted quantities must be inferred from the known observational errors through the dynamic constraints or simplifications therefrom. These σ_i are given by,

$$\begin{aligned}
&\sigma_{\phi_x}=\sigma_{\phi_y}=\frac{\sqrt{2}\,\sigma_\phi}{\Delta S},\\
&\sigma_{\phi_\sigma}=\sigma_T\frac{\partial \ln(p)}{\partial\sigma},\\
&\sigma_{e_u}=\sqrt{2}\,\sigma_u\left[\frac{1}{(\Delta t)^2}-\frac{C^2}{(\Delta S)^2}+\frac{C}{\Delta t\Delta S}\right]^{\frac{1}{2}},\\
&\sigma_{\dot\sigma_k}=\frac{2\Delta\sigma}{\Delta S}\left[\sum_{j=1}^{k}(\sigma_{u_j})^2\right]^{\frac{1}{2}}
\end{aligned} \tag{48}$$

Here S is the average separation between observation sites.

In addition, $\pi_9 = \pi_1$ as terms such as the Taylor series expansion of the Coriolis parameter in product with the wind are considered equal in weight with the wind itself.

Table 1 shows the standard errors of observation for the winds, heights, and temperatures and the RMS errors for the other adjustable meteorological variables. Estimates for the scaler wind speed as functions of elevation angle of the balloon (Fuelberg, 1974) are given in the first two columns. The values for the 20

degree elevation angle compare favorably with the results from Hovermale's (1962) spectral decomposition of meteorological data. RMS values for heights and rawinsonde temperatures are from a composite of methods for estimating measurement error (Achtemeier, 1972).

Table 2 gives the nondimensional precision modulus weights calculated from the various functional relationships of the RMS errors from Table 1. The more accurately measured (estimated) variables receive larger values. Largest weights are accorded the geopotential height followed by the winds and temperatures. The developmental components of the local velocity tendencies receive the smallest weights.

Several modifications in the π_i given in Table 2 were made before the April 10-11 data were subjected to the variational objective analysis. First, the precision modulus weights for levels 9 and 10 of the vertical velocity were assigned large values to require the adjusted vertical velocity to vanish at the top of the domain. Second, the weights for the geopotential were reduced by a factor of 10 because prior studies gave solutions that were forced too strongly toward the geopotential. It is possible that, as a boundary condition, the geopotential has a greater impact upon the the solution than suggested by the magnitude of its precision modulus weight.

4. Evaluation of the Variational Assimilation Model

Three diagnostic criteria were used to evaluate the variational objective analysis. These criteria are, satisfaction of dynamical constraints, adjustment departures from observations, and pattern analysis.

a) Satisfaction of Dynamical Constraints

The method must converge regardless of how well the other criteria are satisfied. But some method must be developed that demonstrates that the analysis does converge. The Sasaki (1970) strong constraint formalism requires that the dynamical constraints; the nonlinear horizontal momentum equations, the hydrostatic equation, the continuity equation, and the thermodynamic equation be satisfied exactly (to within truncation). Recall that the cyclical solution method for solving the Euler-Lagrange equations required the substitution of observed or previously adjusted variables into the forcing functions. As a measure of progress toward convergence, at the end of each cycle, the adjusted variables were averaged with their respective values at the previous adjustment, reintroduced into the dynamical constraints and residuals calculated. It follows that the residuals decrease as the differences between adjusted variables at two successive cycles decrease. The residuals vanish (the

variational objective analysis converges) if the adjusted variables at two successive cycles are the same. A convenient measure of how rapidly the method is converging to a solution is the percent reduction of the initial unadjustment given by,

$$\Delta r(\%) = 100\left(1 - \frac{r^{o} - r^{\tau}}{r^{o}}\right) \qquad (49)$$

Fig. 2 shows how the reductions of the initial RMS differences for the two horizontal momentum equations varies for each pass through the cyclical solution sequence for the eight adjustable levels of the model. The residuals for the u-component momentum equation are approximately halved with each cycle through the fourth cycle. The solution stabilizes to near 99-100 percent reduction of the initial unadjustment except for a 97 percent reduction at the 9th level after eight cycles. The RMS differences for the v-component equation decrease at the first cycle and level off at the second cycle. These differences increase slightly at level 7. Then the residuals decrease monotonically through the eighth cycle with reductions of the initial unadjustment of from 98-99 percent (96 percent at level 9).

There were two reasons why the analysis was done through eight cycles. First, the objective of obtaining near 100 percent reduction in the RMS differences was accomplished for most levels. Second, regardless of the care taken in formulating consistent boundary conditions, there remained deleterious boundary effects that were drawn into the interior of the domain one grid space for

each cycle. The outer three rows of grid points were deleted from the evaluation statistics (see large dashed rectangle in Fig. 1). Therefore, the effects of the boundary conditions entered the evaluation area beginning at the fourth cycle.

The reductions of the initial unadjustment for the integrated continuity equation are shown in the left panel of Fig. 3. The rate of percentage reductions drops off after a large decline at the first pass but still reductions by the eighth pass were mostly between 97-99 percent. The slower convergence at level 9 (92 percent after 8 cycles) and also at level 9 for the horizontal momentum equations may have been the result of large adjustments of the divergent part of the wind required for mass consistency with small vertical velocities in the stratosphere.

The initial unadjustments for the hydrostatic and thermodynamic equations (middle and right panels of Fig. 3) monotonically decreased by about one half at each cycle. The percentage reductions of the RMS differences were mostly near 100 percent at all levels by the eighth cycle.

The satisfaction of constraints test shows that convergence toward a solution was obtained for all levels and for all five dynamic constraints. Therefore, MODEL IIB represents a significant advancement over the MODEL II.

b) Adjustment Departures from Observations

The transferral of the observations to the grid and the modification of the gridded data to satisfy the dynamical constraints is a two-step process. Information from the observations is not available to the second step. Therefore, there is an implicit assumption that the initial gridded fields correctly carry the phenomena described by the observations. This assumption is not strictly true and it is necessary to grid the data with sufficient accuracy so that analysis error does not dominate the first and second derivatives. We have modified the widely used Barnes (1964, 1973) method for gridding meteorological data to yield significant improvement in the accuracy of the gridded data and its derivatives (Achtemeier, 1986, 1989).

In the section under a) above, we showed that the variational objective analysis converges to a solution. Now we seek to find whether the variational method improved upon the unadjusted analysis by adjusting the fields to better fit the original observations.

Consider an "accuracy index" given by the solid lines in Fig. 4. We first calculated two sets of RMS differences, one between values from the unadjusted fields at observation locations and the observations and the second between the adjusted fields and the observations. Then we subtracted from these RMS differences the standard errors of observation for wind components, height, and

temperature listed in Table 1. This means that if the results are zero, the objective analysis has gridded the data to within the standard error of observation for the data. If the results are negative, then the objective analysis has produced a better fit to the observations. Positive values mean that the adjustments have, on the whole, departed farther from the observations than expected. In interpreting these results, it must be kept in mind that the mean winter standard observational error estimates taken from Hovermale's (1962) results do not exactly express the true observational error for this case. Thus, some small departure of either sign from given values should be expected.

The accuracy index for the unadjusted and adjusted heights and temperatures (Figs. 4a and 4b) were within acceptable limits. The index for the adjusted heights was displaced toward the positive, an indication that adjustments away from the observations were necessary to bring the fields into constraint satisfaction. The unadjusted fields of the horizontal velocity components were also within acceptable limits (Figs. 4c and 4d). However, above 800 mb, large positive values for the adjusted velocity components show that the variational analysis produced wind fields that were significantly different from the observations.

The dashed lines in Fig. 4 are the means of the differences between the unadjusted (adjusted) fields interpolated to the observation sites and the observations. Means near zero are expected unless systematic adjustment is required to achieve solution of the variational equations. Means were near zero for

the heights and the temperatures, except for temperatures near the tropopause between 300 mb and 200 mb where systematic adjustments were expected. The means were also near zero for the unadjusted velocity components. However, large systematic adjustments were found for the variationally adjusted velocity components (Figs. 4c and 4d). The u-components were increased on the average 6 m s^{-1} between 500 mb and 300 mb. The v-component systematic reduction was a linear function of pressure. The v-component was on the average decreased by approximately 8 m s^{-1} between 300 mb and 200 mb.

There was no systematic modification of the height fields that could be called upon to explain the adjustments in the velocity fields. An error in the mathematical derivation of the dynamic constraints or in the programming is suspected in these cases. The pattern analysis should provide further insight into the origin of these large systematic adjustments.

c) Pattern Analysis: 00 GMT 11 April 1979

Maps of heights, wind vectors, and temperatures were taken from selected levels within the domain of the variational objective analysis for 00 GMT, 11 April 1979, in order to interpret the statistical results presented in subsections a) and b). Comparisons were made between patterns in the unadjusted initial fields and the adjusted fields. The analyses were done on the synoptic scale however, we note that a mesoscale convective system was located within the high frequency observation area over parts of Texas and Oklahoma.

Heights at 60 m intervals and wind vectors at 300 km intervals are shown in Fig. 5 for 800 mb, 500 mb, and 300 mb. The convention for wind speed is: flag (25 m s^{-1}), barb (5 m s^{-1}), and short barb (2.5 m s^{-1}). At 800 mb, the circulation center has been displaced from its unadjusted location over northwestern Colorado to its adjusted location over eastern Colorado in better agreement with the center of lowest heights. Elsewhere, adjustments in both heights and winds at 800 mb were small (Fig. 6). At 500 mb (Fig. 5), the unadjusted analysis placed a weak short wave trough oriented eastward into Kansas from the parent trough. No trough appears in the wind field over Kansas. Thus, winds blow from high to low heights over Texas and Oklahoma and from low to high heights over Nebraska. The adjusted winds have been turned to more westerly in better agreement with the heights over Texas and

Oklahoma however, east of the Great Plains, the adjusted winds turn to blow toward higher heights. The same pattern of adjustment is also evident at the 300 mb jet stream level. The unadjusted analysis fits the winds with the height field. The adjusted analysis increases the wind speeds and turns the winds more westerly to blow toward higher heights.

The differences between the adjusted and unadjusted fields are shown in Fig. 6 for 500 mb and 300 mb. In general, the variational objective analysis decreased the heights over the northern states and increased the heights over the southern states. The 10 m adjustment over Oklahoma at 500 mb tended to lessen the sharpness of the short wave trough there. Elsewhere, heights were lowered 15-20 m over Montana.

Fig. 6 also shows that an average 5 m s^{-1} westerly component was added to the wind field at 500 mb and an average 10 m s^{-1} northwesterly component was added to the 300 mb wind field. This broad scale adjustment has no apparent relationship to either the height field adjustment or the synoptic weather pattern.

Fig. 7 shows fields of unadjusted and adjusted mean layer temperatures for 750 mb, 450 mb, and 250 mb. The unadjusted patterns at all levels have been preserved by the variational objective analysis. Temperature adjustments were less than one degree at 750 mb and 450 mb. The variational analysis cooled the 250 mb layer by an average of 2C. The unadjusted layer average temperature was too warm across the tropopause and the change was made to make the temperatures consistent with the heights.

The variational objective analysis modified height, temperature, and wind velocity for satisfaction of the dynamic constraints. We now assess how these adjustments have impacted upon derivative quantities such as vorticity, divergence, and vertical velocity that are derived from these basic fields. In addition, the local tendencies of the velocity components and temperature are determined from arithmetic sums of adjusted terms. Patterns of these sensitive variables must be physically realistic when compared with other data sets such as cloud fields, precipitation, and independent measurements of the variable.

Patterns of relative vorticity for the unadjusted and adjusted wind fields are shown in Fig. 8 for 500 mb. The variational objective analysis shifted the vorticity gradient, identifying the area of positive vorticity advection and upward vertical velocity, from over the Texas panhandle to over Oklahoma and Kansas, locations coincident with the mesoscale convective system. Elsewhere, there were only small differences between the unadjusted and adjusted vorticities.

A comparison of the 500 mb vertical velocity patterns (Fig. 9) shows that the variational objective analysis shifted the center of maximum vertical velocity eastward from the Texas panhandle to western Oklahoma in better agreement with the location of the mesoscale convective system located over central Oklahoma and north Texas. The variational analysis also weakened the subsidence area over Nebraska by 2 cm s^{-1}. The subsidence area over Louisiana and eastern Texas in the unadjusted vertical velocities was replaced by

2-4 cm s^{-1} rising motion in the adjusted field. Deep convective precipitation was located within this area (see shaded area in Fig. 9).

Once the variational objective analysis was completed, the developmental components of the local tendencies of velocity components and temperature were recombined with the advective components, redimensionalized, and expressed as 3-hr changes. These 3-hr "adjustment" tendencies were compared with tendencies calculated from 3-hr rawinsonde data collected over the central part of the United States as part of the NASA AVE/SESAME project (see fine dashed grid in Fig. 1). Then "unadjusted" 3-hr tendencies were calculated upon substitution of unadjusted variables into the dynamical constraints and solving for the tendency terms. Inherent in these comparisons is an assumption that the observed 3-hr tendencies are "ground truth". This assumption is not strictly valid for the following reasons. First, it is likely that some of the observations, either at 0000 GMT or at 0300 GMT, were influenced by the mesoscale phenomena within the analysis areas. Second, the unadjusted and adjusted 3-hr tendencies were calculated from 0000 GMT data and are therefore centered at 0000 GMT. These tendencies were compared with the ground truth tendencies that were calculated from observations taken at both 0000-0300 GMT and are therefore centered at 0130 GMT. And third, extrapolation of the local tendencies calculated from the unadjusted and adjusted data has validity only if the time scales of the passage of the weather systems are much greater than

three hours.

Fig. 10 shows fields of the 3-hr u-component tendencies at 800 mb and 500 mb. The observed tendencies show increases in u over Oklahoma and decreases in u over northern Missouri and Iowa. Both unadjusted and adjusted tendencies show similar features but they are shifted to the southwest by about 500 km. Note also that the unadjusted and adjusted tendencies have approximately the same pattern and the centers from the variational objective analysis tend to be slightly larger in magnitude.

The v-component tendencies at 800 mb and 500 mb are shown in Fig 11. Unlike the u-component tendencies, the centers for unadjusted and adjusted tendencies are approximately collocated with the observed centers. The magnitudes of the positive center over Arkansas compare well at 800 mb however the adjusted field shows little correlation with the observed v-tendencies in the western half of the grid. At 500 mb, the centers were mostly collocated however the magnitudes for both the unadjusted and adjusted v-component tendencies were much greater than the observed 3-hr magnitudes - the magnitudes of the adjusted v-component being the largest.

At 300 mb, Fig. 12, both unadjusted velocity component tendencies departed considerably from the observed fields. The adjusted tendencies appeared to be no more correct.

Table 3 gives correlation coefficients between the unadjusted (initial) and observed tendencies and between the adjusted (variational) and observed tendencies for the eight interior levels

of the analysis domain. Somewhat surprisingly, the adjusted correlations were higher than the unadjusted correlations for most levels below 500 mb. In calculating the correlation coefficients that appear in Table 4, we shifted the adjusted and unadjusted tendency fields to the northeast approximately 150 km to account for the 1.5 hr translation of the weather system. The correlations for the shifted tendencies were larger. The variational objective analysis gave improvement over the unadjusted u and v tendencies however, in general the correlations for the adjusted fields were in the range from 0.5-0.8 below 500 mb and were still negative above 400 mb. Results for the temperature tendencies in both tables showed no clear indication of superiority of the adjusted temperatures over the unadjusted temperatures.

5. Discussion

Based upon our experience with developing a basic variational objective analysis technique (Achtemeier et al., 1986) we have derived a new variational objective analysis method that appears to solve all of the problems encountered with earlier versions. These problems included the problem of over-determination noted by Courant (1936), the problem of time consistency that arose upon applying the direct variational method to local tendencies of wind velocity components and temperature, the problem of solving a set of complicated nonlinear partial differential equations, and the problem of decoupling the divergence equation constraint from the

remaining dynamical constraints. This version of the objective analysis contains more equations and requires more complicated solution methods than were necessary for the 1986 version.

The evaluation presented in this report is only preliminary in that it identifies problems with the method but does not determine whether the problems are endemic to the method and therefore degrade data assimilation or whether the problems arise because of correctable errors in the mathematical derivations or the programming.

The satisfactory results of the evaluation are as follows.

1) The method converges for all five dynamic constraints. The divergent part of the wind is strongly coupled in the solution. Convergence after only eight cycles ranged mostly between 98-100 percent of the initial unadjustment with the poorest convergence at the 9th level still at an acceptable 92 percent.

2) The method gave reasonable adjusted fields of heights and temperatures from the standpoint of pattern recognition. The major synoptic weather systems were retained from an accurate initial objective interpolation to the analysis grid. Smaller features such as short waves were also retained. The method did not introduce erroneous wavelengths into the adjusted fields.

3) Sensitive derivative fields such as vorticity and vertical velocity were better located with respect to important

precipitation producing weather systems relative to the unadjusted fields. Gradients of positive vorticity advection were collocated with upward vertical velocity centers.

The unsatisfactory results from the evaluation are as follows.

1) The variational objective analysis systematically increased the zonal component of the wind in a way that caused significant departures from the original observations. These departures appeared to be a function of elevation and of latitude from the grid origin (the largest increases were found in the eastern part of the grid). These departures systematically turned the winds east of the Great Plains to blow from low to high heights.

2) Though at many levels, the patterns were similar, the variational objective analysis greatly overestimated the magnitudes of the local tendencies of the wind components and temperature. Correlations between verification 3-hr tendencies and 3-hr tendencies derived from adjusted data ranged from about 0.5 to 0.8 at levels below 500 mb. Correlations were mostly very small or negative at 200 mb and 300 mb.

The reasons for the unsatisfactory results await a more thorough analysis of the method. The systematic increases in the adjusted wind velocity are suggestive of an error embedded within the mathematical formulas or coding of the programs. We were able

to trace the vary large magnitudes of the tendencies to the advective components. These are relative simple formulations and it has yet to be determined why large advective changes in velocity were found in both the unadjusted and adjusted fields but were not observed.

It could be argued that the large tendencies of the adjusted fields should have been expected given that a mesoscale convective system was within the analysis area during the period 0000-0300 GMT. The variational objective analysis was rerun for 1200 GMT 10 April 1979 data set to test this argument. This period was characterized by the same general synoptic scale long wave trough over the western United States. There were no significant precipitation systems active however. The results showed large magnitude centers of the local tendencies of u and v in both the unadjusted and adjusted fields. Therefore, the finding of large magnitude tendencies within the 0000 GMT 11 April variational analysis was not coincidental with severe weather.

In conclusion, the variational objective analysis represents a mammoth effort in mathematical development and programming. One must question whether, if the problems encountered thus far are solved, the difficulty of the method would limit its use in routine analysis of meteorological data given that there are other nonvariational techniques for blending meteorological data that are being used with success. The answer to the question will in part be delayed until the methods currently in use have been fully applied and evaluated.

Acknowledgments.

This work was supported by the National Aeronautics and Space Administration (NASA) under Grant NAG8-059. The programming efforts of Mrs. Julia Chen are gratefully acknowledged. Mr. Robert Scott prepared the figures.

Appendix A: The Dynamic Constraints

Following Shuman and Hovermale (1968), the horizontal momentum equations and the continuity equation that form the basis of the numerical variational objective analysis/assimilation method are written below as they appear in an arbitrary vertical coordinate and cartesian on a conformal projection of the earth:

$$\frac{\partial u}{\partial t}+m\left(u\frac{\partial u}{\partial x}+v\frac{\partial u}{\partial y}\right)+\dot{\sigma}\frac{\partial u}{\partial \sigma}-fv+m\left(\frac{\partial \phi}{\partial p}\frac{\partial p}{\partial x}+\frac{\partial \phi}{\partial x}\right)+f_u=0 \qquad \text{(A.1)}$$

$$\frac{\partial v}{\partial t}+m\left(u\frac{\partial v}{\partial x}+v\frac{\partial v}{\partial y}\right)+\dot{\sigma}\frac{\partial v}{\partial \sigma}+fu+m\left(\frac{\partial \phi}{\partial p}\frac{\partial p}{\partial y}+\frac{\partial \phi}{\partial y}\right)+f_v=0 \qquad \text{(A.2)}$$

$$\frac{d}{dt}\ln\left(\frac{\partial p}{\partial \sigma}\right)+m\left(\frac{\partial u}{\partial x}+\frac{\partial v}{\partial y}\right)+\frac{\partial \dot{\sigma}}{\partial \sigma}-\left(u\frac{\partial m}{\partial x}+v\frac{\partial m}{\partial y}\right)=0 \qquad \text{(A.3)}$$

The hydrostatic equation is,

$$\frac{\partial \sigma}{\partial p}\frac{\partial \phi}{\partial \sigma}+\frac{RT}{p}=0 \qquad \text{(A.4)}$$

and the thermodynamic equation,

$$\frac{\partial T}{\partial t}+m\left(u\frac{\partial T}{\partial x}+v\frac{\partial T}{\partial y}\right)+\dot{\sigma}\frac{\partial T}{\partial \sigma}-\frac{RT\omega}{c_p p}-\frac{Q}{c_p}=0 \qquad \text{(A.5)}$$

These equations must be subject to several transformations before they can be used in a successful variational method. These transformations are described in the following sections.

A.1 A Nonlinear Vertical Coordinate System

The vertical coordinate is designed to concentrate horizontal variations with the lower coordinate surface to levels below a reference pressure level p^*. The coordinate surfaces above p^* are constant pressure surfaces. The transformation into a nonlinear vertical coordinate was done for the following reasons:

(1) The dynamical equations appear in their simplest form on pressure surfaces. The complex, compensatory terms are confined to levels below p^*.

(2) Vertical interpolation of meteorological observations to coordinate surfaces is not required for pressure surfaces. Further, there is no need to interpolate from sigma coordinates back to pressure surfaces for purposes of interpretation of the variationally adjusted fields of data.

(3) Hydrostatic truncation error and pressure gradient force errors are eliminated on the pressure levels above p^*. The problems of reducing hydrostatic truncation error along

sloping coordinate surfaces are well known (Achtemeier, 1990).

Two curves that are piece wise continuous through the second derivatives make up the nonlinear vertical coordinate. The upper layer relates to pressure by a straight line. Boundary conditions are $\sigma = 0$ at $p = p_u$ and $\sigma = \sigma^*$ at $p = p^*$. This equation is,

$$\sigma=\sigma^*\frac{p-p_u}{p^*-p_u} \tag{A.6}$$

Boundary conditions for the lower curve are $\sigma = 1.0$ at $p = p_s$ and

$$\begin{aligned}\sigma&=\sigma^*\\ \frac{\partial\sigma}{\partial p}&=\frac{\sigma^*}{(p_s-p_u)}\\ \frac{\partial^2\sigma}{\partial p^2}&=0\end{aligned} \tag{A.7}$$

at $p = p^*$. The lower curve, a cubic polynomial, is,

$$\sigma=\beta\,(p-p^*)^3+\sigma^*\frac{p-p_u}{p^*-p_u}, \tag{A.8}$$

where

$$\beta=(1-\sigma^*\frac{p_s-p_u}{p^*-p_u})\,(p_s-p^*)^{-3}. \tag{A.9}$$

Fig. A.1 shows the distribution of coordinate surfaces below 600 mb for the approximate range of surface pressures (800 to 1025 mb) for the smoothed orography of the variational analysis. The reference pressure p^* is 700 mb. These coordinate surfaces tend to

follow constant pressure surfaces at locations away from areas of high elevation. The compression of the coordinate surfaces over higher elevation is clearly evident.

Other variables that are an outcome of the nonlinear vertical coordinate appear elsewhere in the transformation of the dynamic equations. These are:

$$
\begin{aligned}
q_1 &= \frac{-6\beta\,(p-p^*)}{J^2}, \\
q_2 &= \frac{2\alpha J_s}{J}\left(\frac{p-p^*}{p_s-p^*}\right)^3, \\
q_3 &= \frac{1}{Jp}, \\
q_4 &= \frac{J_s}{Jp}\left(\frac{p-p^*}{p_s-p^*}\right)^3, \\
q_5 &= \int_{\sigma_1}^{\sigma_2} q_1\, d\sigma = \frac{J_1}{J_2}.
\end{aligned}
\qquad \text{(A.10)}
$$

where,

$$
\begin{aligned}
\alpha &= \frac{\sigma^*}{p^*-p_u}, \\
J &= 3\beta\,(p-p^*)^2+\alpha, \\
J_s &= 3\beta\,(p_s-p^*)^2+\alpha.
\end{aligned}
$$

It is understood that if $p - p^* < 0$, then $p - p^* \equiv 0$.

Terms in the dynamic equations that must be transformed are as follows:

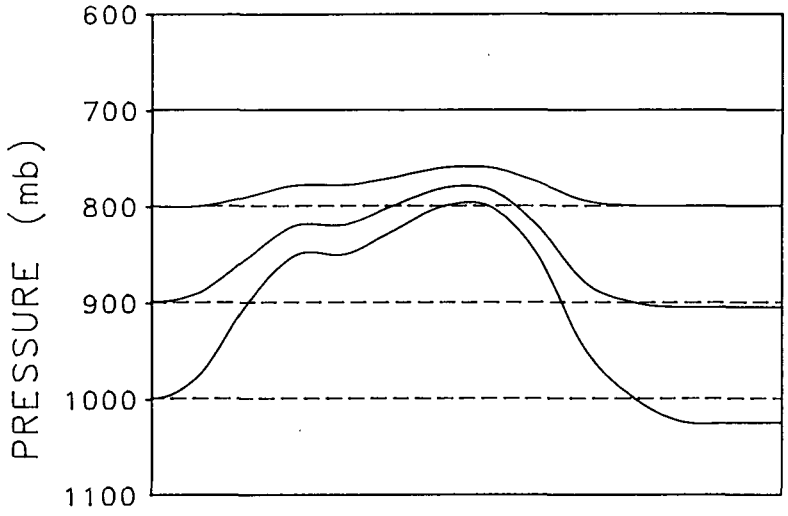

Fig. A.1 Distribution of coordinate surfaces below 800 mb.

(1) The pressure gradient force terms of the horizontal momentum equations (A.1 and A.2) take the form,

$$m\left(\frac{\partial \phi}{\partial p}\frac{\partial p}{\partial x}+\frac{\partial \phi}{\partial x}\right)=m\left(RT\frac{\partial \ln p}{\partial x}+\frac{\partial \phi}{\partial x}\right) \qquad \text{(A.11)}$$

(2) The first term of the continuity equation transforms into

$$\frac{d}{dt}\ln\frac{\partial p}{\partial \sigma}=q_1\dot{\sigma}+q_2\omega_s \qquad \text{(A.12)}$$

(3) The hydrostatic equation transforms to,

$$\frac{\partial \phi}{\partial \sigma}+T\frac{\partial \ln p}{\partial \sigma}=0 \qquad \text{(A.13)}$$

(4) The fourth term of the thermodynamic equation (5) becomes,

$$\frac{RT\omega}{c_p p}=\frac{RT}{c_p}\left(q_3\dot{\sigma}+q_4\omega_s\right) \qquad \text{(A.14)}$$

A.2 Reduction of Terrain Impacts upon Analysis

Small hydrostatic residuals and related pressure gradient force errors that plague numerical models written in terrain-following coordinates have been well documented. Much larger errors can be generated upon subjecting the pressure gradient terms of the horizontal momentum equations to the variational operations. The variational operator separates the two pressure gradient terms and combines the large now uncompensated terms with terms from the other equations. The terrain terms, for which the nonmeteorological part may exceed 90 percent of the magnitude of

the term, can dominate the adjustment. A test found that these terms generated large error that caused the variational method to diverge.

The above problem may be avoided if the hydrostatic terms are partitioned to isolate the terrain part so that the variation can be applied to only the meteorological "signal". Note that a partition not a transforation is done. There is no change in the vertical coordinate.

The equations were nondimensionalized following the methodology of Charney (1948) and Haltiner (1971). The resulting nondimensional variables contain the "whole" signal. The geopotential height and temperature are partitioned into terrain, reference, meteorological, and residual categories according to,

$$( )_w = ( )_T + ( )_R + ( )^o + [( ) - ( )^o] \qquad \text{(A.15)}$$

In addition, the "whole" pressure is partitioned into terrain and reference parts according to

$$p_w = p_T + p_R \qquad \text{(A.16)}$$

The hydrostatic equation is partitioned into four groups of terms. These are:

Terrain,

$$[(\frac{p_w}{p_R} - 1) \frac{\partial \phi_w^o}{\partial \sigma} + \frac{\partial \phi_T}{\partial \sigma} + \frac{T_w^o}{p_R} \frac{\partial \ln p_T}{\partial \sigma}] \qquad \text{(A.17)}$$

Reference,

$$[\frac{\partial \phi_R}{\partial \sigma} + \gamma T_R] \tag{A.18}$$

Meteorological,

$$[\frac{\partial \phi}{\partial \sigma} + \gamma T] \tag{A.19}$$

Residual,

$$[(\frac{p_w}{p_R} - 1)\frac{\partial}{\partial \sigma}(\phi - \phi^o) + \frac{T - T^o}{p_R}\frac{\partial \ln p_T}{\partial \sigma}] \tag{A.20}$$

where,

$$\gamma = \frac{\partial \ln p_R}{\partial \sigma}$$

Non-derivative p_w and p_R in (A.17) and (A.20) are layer mean pressures which must be accurately known for the partition to be successful. After some experimentation, it was found that, given the pressures at the top and the bottom of the layer, the average of the arithmetic mean plus twice the geometric mean,

$$p = \frac{0.5(p_t + p_b) + 2\sqrt{p_t p_b}}{3}$$

yields accurate layer mean pressure. The superscript zero identifies observed variables. These are not subject to the variational operations.

Upon specification of p_R (p_R = 1000, 900, 800 mb), p_T is known through (A.16). Therefore, (A.17) can be solved for the terrain

height ϕ_T. ϕ_R is found from the level average of height after the removal of ϕ_T. Remaining reference variables are obtained through (A.18) and the meteorological variables are found from (A.15). The residual group (A.20) exist through small modifications in ϕ that result from the variational operation. These terms are typically two orders of magnitude smaller than the meteorological terms. If these terms are represented by β, then the hydrostatic equation that is subject to the variational operation is,

$$\frac{\partial \phi}{\partial \sigma} + \gamma T + \beta = 0 \qquad \text{(A.21)}$$

Now the pressure gradient terms of the horizontal momentum equations can be partitioned to separate the terrain part from the meteorological part that is subject to the variational operations. The modified nondimensional pressure gradient term is,

$$\frac{\partial \phi}{\partial x} + T\frac{\partial \ln p}{\partial x} = \frac{\partial \phi}{\partial x} + \eta_x \qquad \text{(A.22)}$$

where,

$$\eta_x = (T - T^o)\frac{\partial \ln p_T}{\partial x} + \frac{\partial \phi_T}{\partial x} + T_w^o \frac{\partial \ln p_T}{\partial x}$$

A.3 Partition of the Local Tendencies of u and v

Local changes in the horizontal velocity components result from translation of existing disturbances and development.

Consider that the local change in the u-component of the wind for a moving weather system is,

$$\frac{\partial u}{\partial t} = -c\cdot\nabla u + \frac{du}{dt} \qquad \text{(A.23)}$$

where c is the velocity of an advective or steering current (Fjortoft, 1952) usually a smoothed middle tropospheric wind. Let $u = u_0 + u'$ where u_0 is the u-component of the steady part of the circulation and u' arises from development. Then,

$$\frac{\partial u}{\partial t} = -c\cdot\nabla u_o + \left(\frac{du'}{dt} - c\cdot\nabla u'\right)$$

The first term is the local change in u caused by translation of the steady part of a disturbance. The second term is the local change of u from development. Note that the vertical advection of u is considered part of development.

The use of the advective current throughout the troposphere is valid because most synoptic systems tend to maintain vertical structure. Any changes in vertical structure are assumed to be the result of development. However, the variational operations require that the adjustments be done on total velocity components. Therefore, we represent the local tendency of u by (A.23). The total derivative, an approximate developmental component, is defined as a new dependent variable, $\epsilon_u = du/dt$ ($\epsilon_v = dv/dt$).

A.4 The Dynamic Constraints

Subjecting the dynamic equations (A.1) - (A.5) to the required transformations yields the following constraints: For the horizontal momentum equations,

$$R_o[\epsilon_u + m(u-c_x)\frac{\partial u}{\partial x} + m(v-c_y)\frac{\partial u}{\partial y} + R_o\dot{\sigma}\frac{\partial u}{\partial \sigma}] - (1+R_1C)v + (1+R_1K)(\frac{\partial \phi}{\partial x} + \eta_x) + f_u = 0 \quad \text{(A.24)}$$

$$R_o[\epsilon_v + m(u-c_x)\frac{\partial v}{\partial x} + m(v-c_y)\frac{\partial v}{\partial y} + R_o\dot{\sigma}\frac{\partial v}{\partial \sigma}] + (1+R_1C)u + (1+R_1K)(\frac{\partial \phi}{\partial y} + \eta_y) + f_v = 0 \quad \text{(A.25)}$$

As part of the nondimensionalization, the Coriolis parameter and the map scale factor have been expanded into a Taylor series. Thus, $f = 1 + R_1C$ and $m = 1 + R_1K$ where $R_1 = 0.1$.

The continuity equation will become an integrated constraint,

$$\int q_5(\frac{\partial u}{\partial x} + \frac{\partial v}{\partial y})\,d\sigma + (\dot{\sigma} - \dot{\sigma}_0) + \int q_5[\frac{Lh}{Hl}q_2\omega_s + R_1K(\frac{\partial u}{\partial x} + \frac{\partial v}{\partial y}) - R_1(u\frac{\partial K}{\partial x} + v\frac{\partial K}{\partial y})]\,d\sigma = 0 \quad \text{(A.26)}$$

The hydrostatic and thermodynamic equations are,

$$\frac{\partial \phi}{\partial \sigma} + \gamma T + \beta = 0 \quad \text{(A.27)}$$

$$R_o\left[\epsilon_T+m\left(u\frac{\partial T}{\partial x}+v\frac{\partial T}{\partial y}\right)+\dot{\sigma}\left(\frac{\partial T}{\partial \sigma}-\kappa q_3 T\right)\right.$$
$$\left.-\kappa q_4 \omega_s\left(\frac{R_o}{F}T_R+T\right)\right]+\dot{\sigma}\sigma_\sigma-\frac{Q^*}{C_p}=0 \qquad \text{(A.28)}$$

where,

$$\sigma_\sigma=\frac{R_o^2}{F}\left(\frac{\partial T_R'}{\partial \sigma}-\kappa q_3 T_R'\right)$$

is the static stability. Here F is the Froude number and Q^* carries nondimensionalization constants. In addition,

$$\kappa=\frac{R}{C_p}$$

$$\epsilon_T=\frac{dT}{dt}$$

where the latter is introduced as a dependent variable.

Appendix B: Finite Difference Equations for the Dynamic Constraints

The dynamic equations will be written in centered differences on an Arakawa D grid (Mesinger and Arakawa, 1976). Fig. B1 shows the distribution of variables on the staggered grid. Anthes and Warner (1978) define the horizontal finite difference operators and the finite averaging operators as

$$\begin{aligned} \alpha_x &\equiv (\alpha_{i+1/2,j}-\alpha_{i-1/2,j})/\Delta x \\ \alpha_y &\equiv (\alpha_{i,j+1/2}-\alpha_{i,j-1/2})/\Delta y \\ \overline{\alpha}^x &\equiv (\alpha_{i+1/2,j}+\alpha_{i-1/2,j})/2 \\ \overline{\alpha}^y &\equiv (\alpha_{i,j+1/2}+\alpha_{i,j-1/2})/2 \end{aligned} \tag{B.1}$$

The i are the east-west indices, the j are the north-south indices as defined at the grid origin located at the lower left corner of the grid. In addition, the vertical differences and averages are defined by

$$\begin{aligned} \alpha_\sigma &\equiv (\alpha_{k+1/2}-\alpha_{k-1/2})/\Delta\sigma \\ \overline{\alpha}^\sigma &\equiv (\alpha_{k+1/2}+\alpha_{k-1/2})/2 \end{aligned} \tag{B.2}$$

The finite difference equations for the horizontal momentum equations are,

$$M_6 = -v+\phi_x+F_5=0 \tag{B.3}$$

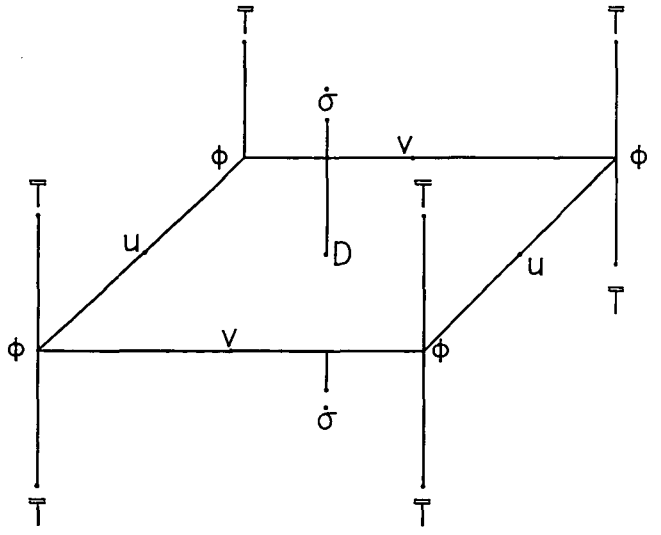

Fig B1. The grid template for the variational assimilation model.

$$M_1 = -F_5 + R_o [\overline{\epsilon_u}^{xy} + \overline{m}^x (\overline{u - c_x})^{xy} \overline{u}_x^y + \overline{m}^x (v - c_y) \overline{u}_y^x + R_o \overline{\sigma}^{y\sigma} \overline{u}_\sigma^{xy\sigma}] - R_1 \overline{C}^x v + R_1 \overline{K}^x \phi_x + (1 + R_1 \overline{K}^x) \eta_x + f_u = 0 \quad \text{(B.4)}$$

$$M_7 = u + \phi_y + F_6 = 0 \quad \text{(B.5)}$$

$$M_2 = -F_6 + R_o [\overline{\epsilon_v}^{xy} + \overline{m}^y (u - c_x) \overline{v}_x^y + \overline{m}^y (\overline{v - c_y})^{xy} \overline{v}_y^x + R_o \overline{\sigma}^{x\sigma} \overline{v}_\sigma^{xy\sigma}] + R_1 \overline{C}^y u + R_1 \overline{K}^y \phi_y + (1 + R_1 \overline{K}^y) \eta_y + f_v = 0 \quad \text{(B.6)}$$

The continuity equation is

$$M_3 = \int q_5 (u_x + v_y) \, d\sigma + (\dot{\sigma} - \dot{\sigma}_o) + \int q_5 F_7 \, d\sigma = 0 \quad \text{(B.7)}$$

$$F_7 = \int [\frac{Lh}{Hl} q_2 \omega_s + R_1 \overline{K}^{xy} (u_x + v_y) - R_1 (\overline{u}^x \overline{K}_x^y + \overline{v}^y \overline{K}_y^x)] \, d\sigma \quad \text{(B.8)}$$

The hydrostatic and thermodynamic equations are,

$$M_4 = \phi_\sigma + \gamma T + \beta = 0 \quad \text{(B.9)}$$

$$M_5 = R_o [\epsilon_T + \overline{m}^{xy} \overline{u}^{x\sigma} \overline{T}_x^y + \overline{m}^{xy} \overline{v}^{y\sigma} \overline{T}_y^x + \dot{\sigma} (\overline{T}_\sigma^{xy\sigma} - \kappa \overline{q_3}^{xy} \overline{T}^{xy}) - \kappa \overline{q_4}^{xy} \omega_s (\frac{R_o}{F} T_R + \overline{T}^{xy})] + \dot{\sigma} \sigma_\sigma - \frac{Q^*}{c_p} = 0 \quad \text{(B.10)}$$

The seven dynamic equations are referenced at, respectively, M_1 and M_6 at v, M_2 and M_7 at u, M_3 at D, M_4 at T, and M_5 at the vertical velocity.

Appendix C: The Euler-Lagrange Equations

The gridded fields of meteorological data to be modified are meshed with the dynamical equations through Sasaki's (1970a) variational operations. To simplify the derivations, the frictional terms in the horizontal momentum equations and the diabatic heating term in the thermodynamic equation were set to zero.

Early experiments with this method found that the divergent part of the wind was decoupled from the adjustment with the result that the continuity equation was not satisfied. Attempts to readjust the winds through a subsidiary variational formulation that satisfied the continuity equation were not successful. The vertical velocity tended to "drift" with the result that the thermodynamic equation was not satisfied.

Analysis of the problem revealed that the divergent part of the wind could be coupled with the variational adjustment if an additional constraint was satisfied. The adjusted variables must satisfy a particular solution of the integrated vorticity equation. The integrated divergence and the integrated vorticity theorem must vanish at the top of the model domain. This requirement is met if F_5 and F_6 are made dependent variables and M_3 is modified to

$$M_3 = -q_5 (F_{6x} - F_{5y}) \Delta\sigma + (\dot{\sigma} - \dot{\sigma}_o) + q_5 F_7 \Delta\sigma = 0 \qquad \text{(C.1)}$$

In addition,

$$M_6 = -v + \phi_x + F_5 = 0 \tag{C.2}$$

$$M_7 = u + \phi_y + F_6 = 0 \tag{C.3}$$

The finite difference analog of the adjustment functional is,

$$\tilde{F} = \Delta x \Delta y \sum_i \sum_j a_i b_j I_{i,j} \tag{C.4}$$

The integrand, $I_{i,j}$ is

$$\begin{aligned} I = & \pi_1 (u-u^o)^2 + \pi_1 (v-v^o)^2 + \pi_2 (\dot{\sigma}-\dot{\sigma}^o)^2 \\ & + \pi_3 (\phi-\phi^o)^2 + \pi_4 (T-T^o)^2 + \pi_5 (\phi_x-\phi_x^o)^2 \\ & + \pi_5 (\phi_y-\phi_y^o)^2 + \pi_6 (\phi_\sigma-\phi_\sigma^o)^2 + \pi_7 (\epsilon_u-\epsilon_u^o)^2 \\ & + \pi_7 (\epsilon_v-\epsilon_v^o)^2 + \pi_8 (\epsilon_T-\epsilon_T^o)^2 + \pi_9 (F_5-F_5^o)^2 \\ & + \pi_9 (F_6-F_6^o)^2 + 2 \sum_{i-1}^{7} \lambda_i M_i \end{aligned} \tag{C.5}$$

The weights, π_i, are Gauss' precision moduli (Whittaker and Robinson, 1926). The gridded initial variables (u^o, v^o, σ^o, Φ^o, T^o, ϵ_u^o, $_v^o$, F_5^o, F_6^o) enter in a least squares formulation and receive π_i according to their relative accuracies. The strong constraints to be satisfied exactly are introduced through the Lagrangian multipliers λ_i.

Objectively modified meteorological variables are determined by requiring the first variation on F to vanish. A necessary condition for the existence of a stationary set is that the functions are determined from the domain of admissible functions as solutions of the Euler-Lagrange equations. The variation is to be

carried out at every point (r,s) within the grid. Thus, upon setting the weights $a_i = b_j = 1$ and differentiating the integrand (C.5) with respect to the arbitrary variable $\alpha_{r,s}$, the Euler-Lagrange operator in finite differences is

$$\frac{\partial I_{i,j}}{\partial \alpha_{r,s}} - I_{\alpha_{i,j}} \frac{\partial \alpha_{i,j}}{\partial \alpha_{r,s}} - I_{\alpha_{i,j}} \delta_r^i \delta_s^j = 0 \qquad \text{(C.6)}$$

Each term in $I_{i,j}$ that contains an overbar term, that is, each term in M_i [(B.4), (B.6), (B.9), (B.10), (C.1) - C.3)] produces an overbar term when subjected to the operations specified by (C.6). Multiplicate overbar terms such as $(\bar{xy})$ are treated having no overbar so that fewer grid points are required to express these terms in the Euler-Lagrange equations.

The Euler-Lagrange equations resulting from the operations specified by (C.6) are

$$\pi_1 u + \lambda_6 + F_1 = 0 \qquad \text{(C.7)}$$

$$\pi_1 v - \lambda_5 + F_2 = 0 \qquad \text{(C.8)}$$

$$\pi_2 \dot{\sigma} + \lambda_3 + F_3 = 0 \qquad \text{(C.9)}$$

$$\overline{\pi}_5^{xy}\nabla^2\phi+\overline{\pi}_6^{\sigma}\phi_{\sigma\sigma}+\pi_{5x}\overline{\phi}_x^x+\pi_{5y}\overline{\phi}_y^y+\pi_{6\sigma}\overline{\phi}_{\sigma}^{\sigma}$$
$$-\pi_3\phi+\lambda_{5x}+\lambda_{6y}+\lambda_{4\sigma}+F_4=0 \qquad \text{(C.10)}$$

$$\pi_4 T+\gamma\lambda_4+F_8=0 \qquad \text{(C.11)}$$

$$\pi_7(\epsilon_u-\epsilon_u^o)+R_o\lambda_1=0 \qquad \text{(C.12)}$$

$$\pi_7(\epsilon_v-\epsilon_v^o)+R_o\lambda_2=0 \qquad \text{(C.13)}$$

$$\pi_8(\epsilon_T-\epsilon_T^o)+R_o\lambda_7=0 \qquad \text{(C.14)}$$

$$\pi_9(F_5-F_5^o)-\lambda_1+\lambda_5-\Delta\sigma(q_5\overline{\lambda}_3^{\sigma})_y=0 \qquad \text{(C.15)}$$

$$\pi_9(F_6-F_6^o)-\lambda_2+\lambda_6+\Delta\sigma(q_5\overline{\lambda}_3^{\sigma})_x=0 \qquad \text{(C.16)}$$

Variation on the Lagrange multipliers restores the original constraints [(B.4), (B.6), (B.9), (B.10), (C.1) - C.3)].

The forcing functions, F_1 - F_4 contain the following:

$$F_1=-\pi_1 u^o-\Delta\sigma\lambda_{3x}+R_1\overline{C}^y\lambda_2+R_o\{\overline{m}^y\overline{\lambda}_1^{xy}\overline{u}_x^x+\overline{m}^y\lambda_2\overline{v}_x^y$$
$$-[\overline{m}^{xy}\overline{\lambda}_1^y(\overline{u-c_x})^x]_x-[\overline{m\lambda_1(v-c_y)}^x]_y-R_o(\overline{\sigma}^x\overline{\lambda}_1^{xy\sigma})_{\sigma} \qquad \text{(C.17)}$$
$$+\overline{m}^y(\overline{\lambda_7 T_x^y})^{x\sigma}\}-R_1[(\lambda_3\overline{K}^{xy})_x+\lambda_3\overline{K}_x^{xy}]$$

$$F_2 = -\pi_1 V^{o} - \Delta\sigma\lambda_{3y} - R_1\overline{C}^{x}\lambda_1 + R_o\{\overline{m}^{x}\lambda_1\overline{u}_y^{x} + \overline{m}^{x}\overline{\lambda}_2^{xy}\overline{v}_y^{y}$$
$$- [m\overline{\lambda_2(u-c_x)}^{y}]_x - [\overline{m}^{xy}\overline{\lambda}_2^{x}(\overline{v-c_y})^{y}]_y - R_o(\overline{\sigma}^{y}\overline{\lambda}_2^{xy\sigma})_\sigma \quad (C.18)$$
$$+\overline{m}^{x}\overline{(\lambda_7\overline{T}_y^{x})}^{y\sigma}\} - R_1[(\lambda_3\overline{K}^{xy})_y + \lambda_3\overline{K}_y^{xy}]$$

$$F_3 = -\pi_2\dot{\sigma}^{o} + \lambda_5\sigma_\sigma + R_o\lambda_5(\overline{T}_\sigma^{xy\sigma} - \kappa\overline{q}_3^{xy}\overline{T}^{xy}) + R_o^2(\overline{\lambda}_1^{y\sigma}\overline{u}_\sigma^{x} + \overline{\lambda}_2^{x\sigma}\overline{v}_\sigma^{y}) \quad (C.19)$$

$$F_4 = \pi_3\phi_o - \pi_5\nabla^2\phi^{o} - \pi_6\phi_{\sigma\sigma}^{o} - \pi_{5x}\overline{\phi}_x^{ox} - \pi_{5y}\overline{\phi}_y^{oy} - \pi_{6\sigma}\overline{\phi}_\sigma^{o\sigma} + R_1K(\lambda_{1x} + \lambda_{2y}) \quad (C.20)$$

In addition, the forcing function F_8 is,

$$F_8 = -\pi_4 T^{o} - R_o[(\overline{m}^{x}\overline{u}^{x}\overline{\lambda_7^\sigma})_x^y + (\overline{m}^{y}\overline{v}^{y}\overline{\lambda_7^\sigma})_y^x + (\overline{\sigma\lambda_7})_\sigma^{xy\sigma} + \kappa q_3(\overline{\sigma\lambda_7})^{xy}$$
$$+\kappa q_4(\overline{\omega_s\lambda_7})^{xy}] \quad (C.21)$$

We observe that the forcing functions contain the nonlinear terms of their respective equations. Further, the forcing functions consist of terms that are either observed and therefore not adjusted, or are multiplied by R_o or R_1. These equations may be therefore linearized and a solution obtained through a cyclical method as follows. Terms multiplied by R_o or R_1 are expressed with observed variables at the first cycle, and are expressed by previously adjusted variables at higher cycles. Therefore the forcing functions are known at each cycle. This solution method is valid for the latitudes and motion scales for which the Rossby number is less than one.

The set of equations [(B.4), (B.6), (B.9), (B.10), (C.1) - C.3), (C.7) - (C.16)] are the linear algebraic and partial differential equations to be solved. Variables may be eliminated to reduce the number of equations to three diagnostic equations in vorticity, divergence, geopotential. Eliminate λ_4, λ_5, λ_6, and T between, respectively, (B.9), (C.10) and (C.11); (C.8) and (C.15), and (C.7) and (C.16). Next, eliminate $_3$ between (C.9) and (C.15) and (C.16). Then, λ_1 and λ_2 may be eliminated between (C.12) and (C.13) and (C.10), (C.15) and (C.16). If M_1 and M_2 are rewritten, pulling out the ϵ_u and ϵ_v terms and designating the remaining terms as f_5 and f_6, respectively, then ϵ_u and ϵ_v may be eliminated by substituting (C.12) and (C.13) into (C.15) and (C.16). Finally, letting $D = u_x + v_y$, the vertical velocity can be eliminated between (C.1) and (C.15) and (C.16). Performing the above operations reduces the Euler-Lagrange equation set to the following five equations:

$$-v+\phi_x+F_5=0 \tag{C.22}$$

$$u+\phi_y+F_6=0 \tag{C.23}$$

$$\pi_1 v+(\pi_9+\frac{\pi_7}{R_o^2})F_5-(\Delta\sigma)^2[\overline{(Q_5^2\pi_2)^{\sigma}D}]_y+G_{1y}+G_3=0 \tag{C.24}$$

C-2

$$-\pi_1+(\pi_9+\frac{\pi_7}{R_o^2})F_6+(\Delta\sigma)^2[\overline{(q_5^2\pi_2)^{\sigma}D}]_x-G_{1x}-G_2=0 \qquad (C.25)$$

$$\begin{aligned}&\overline{\pi}_5^{xy}\nabla^2\phi+\overline{\pi}_6^{\sigma}\phi_{\sigma\sigma}+\pi_{5x}\overline{\phi}_x^x+\pi_{5y}\overline{\phi}_y^y+\pi_{6\sigma}\overline{\phi}_{\sigma}^{\sigma}\\&-\pi_3\phi+(\pi_1 v)_x-(\pi_1 u)_y+G_4=0\end{aligned} \qquad (C.26)$$

where the forcing functions, G_1 - G_4 are given by:

$$G_1=\Delta\sigma[q_5\overline{F}_3^{\sigma}+q_5\pi_2\dot{\sigma}^{o}-q_5\overline{\pi}_2^{\sigma}F7\Delta\sigma]$$

$$G_2=\pi_9F_6^{o}+\frac{\pi_7}{R_o^2}(f_6+R_o\varepsilon_v^{o})+F_1$$

$$G_3=-\pi_9F_5^{o}-\frac{\pi_7}{R_o^2}(f_5+R_o\varepsilon_u^{o})+F_2$$

$$G_4=F_{2x}-F_{1y}+(\frac{\pi_4\beta}{\gamma^2}+\frac{\pi_4T^{o}}{\gamma})_{\sigma}+F_4$$

We are now in a position to substitute (C.22) and (C.23) into (C.24) and (C.25) to eliminate F_5 and F_6. We make note that the substitution generates the following combination of precision modulus weights,

Further, we note that all of these precision moduli vary horizontally with horizontal variations in π_1. Thus, if,

$$\pi_{10}=\pi_1+\pi_9+\frac{\pi_7}{R_o^2}; \quad \pi_{11}=\pi_9+\frac{\pi_7}{R_o^2}.$$

$\pi_1(x,y,\sigma)=\pi_1(\sigma)f(x,y)$, and the horizontal variations of π_7 and π_9 also vary as $f(x,y)$, then by dividing all precision moduli by $f(x,y)$, the horizontal variations of π_{10} and π_{11} may be removed without changing the relative relationships between the weights. With these modifications, the Euler-Lagrange equations (C.24) and (C.25) may be combined to form a divergence equation,

$$\nabla^2[(\Delta\sigma)^2 q_5^2 \pi_2 D]-\pi_{10}D=\nabla^2 G_1+G_{2x}+G_{3y} \tag{C.27}$$

The vorticity formed from (C.24) and (C.25) is,

$$\pi_{10}\zeta-\pi_{11}\nabla^2\phi=G_{2y}-G_{3x} \tag{C.28}$$

Substitution of the vorticity between (C.26) and (C.28) leaves a diagnostic equation in geopotential,

$$\left(\overline{\pi}_5^{xy}+\pi_1\frac{\pi_{11}}{\pi_{10}}\right)\nabla^2\phi+\left(\overline{\pi}_6^{\sigma}+\frac{\pi_4}{\gamma^2}\right)\phi_{\sigma\sigma}+\pi_{5x}\overline{\phi}_x^x+\pi_{5y}\overline{\phi}_y^y+\left(\pi_{6\sigma}+\frac{\pi_4}{\gamma^2}\right)\overline{\phi}_\sigma^\sigma-\pi_3\phi$$
$$=-G_4-\frac{\pi_1}{\pi_{10}}(G_{2y}-G_{3x}) \tag{C.29}$$

Equations (C.27) - (C.29) form the three diagnostic equations that must be solved for a successful variational adjustment. All terms to the right of the equal sign are forcing functions that contain either unadjusted initial variables and/or variables that have been adjusted at the last iteration. (C.29) is solved first to get the geopotential height. Then the divergence and vorticity are

obtained through (C.27) and (C.28).

Appendix D: Boundary Conditions

The variational theory specifies natural boundary conditions that are consistent with the Euler-Lagrange equations. If it is assumed that there are no adjustments in the data along the boundaries, then the boundary conditions may be specified. In the latter case, the Lagrange multipliers, λ_i, are zero at the boundaries and the initial unadjusted values are used for the boundary conditions.

Initially, the Euler-Lagrange equations were solved with specified boundary conditions. These boundary conditions forced high frequency waves into the solutions for the velocity components near the boundaries. Divergences calculated from these velocity components gave large erroneous vertical velocities. We therefore returned to the natural boundary conditions.

The Euler-Lagrange operator for natural boundary conditions is,

$$\frac{\partial I}{\partial\left(\frac{\partial f_i}{\partial x_j}\right)}=0 \qquad \text{(D.1)}$$

Performing the operation specified by (D.1) yields the following expressions for the boundary conditions on Φ

$$\pi_5(\phi_x-\phi_x^{\circ})+\lambda_5+R_1K\lambda_1=0 \qquad \text{(D.2)}$$

$$\pi_5(\phi_y-\phi_y^o)+\lambda_6+R_1K\lambda_2=0 \tag{D.3}$$

$$\pi_6(\phi_\sigma-\phi_\sigma^o)+\lambda_4=0 \tag{D.4}$$

The terms multiplied by R_1 come from the constraints, M_1 and M_2. These equations can be solved for the Φ boundary conditions subject to substitutions for the λ_i through the Euler-Lagrange equations (22)-(35) in the text. The lateral boundary conditions for the x- and y-boundaries are, respectively,

$$\begin{aligned}(\pi_{10}\pi_5+\pi_{13})\phi_x-\pi_{10}\pi_5\phi_x^o+\frac{\pi_{13}}{\pi_1}F_2+\pi_9\pi_{12}F_5^o+\pi_{12}\Delta\sigma(Q\lambda_3)_y\\ +\frac{\pi_7}{R_o}(1+\pi_{12})\left(\frac{f_5}{R_o}+\epsilon_u^o\right)=0\end{aligned} \tag{D.5}$$

$$\begin{aligned}(\pi_{10}\pi_5+\pi_{13})\phi_y-\pi_{10}\pi_5\phi_y^o-\frac{\pi_{13}}{\pi_1}F_1+\pi_9\pi_{12}F_6^o-\pi_{12}\Delta\sigma(Q\lambda_3)_x\\ +\frac{\pi_7}{R_o}(1+\pi_{12})\left(\frac{f_6}{R_o}+\epsilon_v^o\right)=0\end{aligned} \tag{D.6}$$

where,

$$\pi_{10}=\frac{\pi_9+\pi_1+\frac{\pi_7}{R_o}}{\pi_1},$$

$$\pi_{11}=\pi_9+\frac{\pi_7}{R_o},$$

$$\pi_{12}=1-\frac{R_1K}{R_o}\frac{\pi_7}{\pi_1},$$

$$\pi_{13}=\pi_{11}\pi_{12}+\frac{\pi_7}{R_o}\pi_{10}.$$

Several observations may be made with regard to (D.5) and (D.6).

(1) F_1, F_2, λ_3, f_5, and f_6 all contain terms that are updated at each cycle. Thus it is possible to update the boundary conditions as the interior fields are being adjusted.

(2) These forcing functions contain nonlinear terms that cannot be calculated at the boundaries unless derivatives are extrapolated across the boundaries. Therefore, the boundary equations may be simplified by setting $\lambda_1 = \lambda_2 = \lambda_3 = 0$ at the boundaries. It follows therefore, that

$$F_1 = -\pi_1 u^o, \quad F_2 = -\pi_1 v^0, \quad F_3 = -\pi_2 \dot{\sigma}^o$$

(3) From (22) and (29),

$$Q\Delta\sigma\,(D+F_7) + \frac{\lambda_3}{\pi_2} + \dot{\sigma}^o - \dot{\sigma}_0 = 0 \qquad \text{(D.7)}$$

Given that it is the gradient of λ_3 that appears in (D.5) and (D.6) it follows from (D.7) that gradient of the divergence must be specified, or in other words, the divergence must be specified along at least two boundary grid rows or columns in order that the gradient of λ_3 vanish in the Φ boundary equations.

(4) π_7 is at least two orders of magnitude smaller than the remaining precision moduli. Neglecting π_7 leads to the following simplifications,

The equations for the lateral boundary conditions on Φ are thus,

$$\pi_{10}=\frac{\pi_9+\pi_1}{\pi_1},\quad \pi_{11}=\pi_{13}=\pi_9,\quad \pi_{12}=1$$

$$\begin{aligned}(\pi_5+\frac{\pi_1\pi_9}{\pi_1+\pi_9})\phi_x-\pi_5\phi_x^o-\frac{\pi_1\pi_9}{\pi_1+\pi_9}(u^o-F_5^o)=0\\(\pi_5+\frac{\pi_1\pi_9}{\pi_1+\pi_9})\phi_y-\pi_5\phi_y^o+\frac{\pi_1\pi_9}{\pi_1+\pi_9}(u^o+F_6^o)=0\end{aligned}\qquad (D.8)$$

The boundary conditions for u and v may be found by solving the same set of equations used for finding the Φ boundary conditions but for u and v. The results are,

$$\begin{aligned}(\pi_5+\pi_1\frac{\pi_5+\pi_9}{\pi_9})v-\pi_5(\phi_x^o-F_5^0)-\pi_1\frac{\pi_5+\pi_9}{\pi_9}v^o=0\\(\pi_5+\pi_1\frac{\pi_5+\pi_9}{\pi_9})u+\pi_5(\phi_y^o+F_6^o)-\pi_1\frac{\pi_5+\pi_9}{\pi_9}u^o=0\end{aligned}\qquad (D.9)$$

REFERENCES

Achtemeier, G. L., 1990: Reducing hydrostatic truncation error in a meso-beta boundary layer model. (Accepted for publication in Mon. Wea. Rev.)

Achtemeier, G. L., 1989: Modification of a Successive Corrections Objective Analysis for Improved Higher Order Calculations. Mon. Wea. Rev., 117, 78-86.

Achtemeier, G. L., 1986: The impact of data boundaries upon a successive corrections objective analysis of limited-area data sets. Mon. Wea. Rev., 114, 40-49.

Achtemeier, G. L., 1979. Evaluation of operational objective streamline methods. Mon. Wea. Rev. 107, 198-206.

Achtemeier, G. L., 1975: On the Initialization problem: A variational adjustment method. Mon. Wea. Rev., 103, 1090-1103.

Achtemeier, G. L., 1972: Variational initialization of atmospheric fields - a quasi-geostrophic diagnostic model. Ph.D. Dissertation, Tallahassee, Florida State University, 101-103.

Achtemeier, G. L., H. T. Ochs, III, S. Q. Kidder, R. W. Scott, J. Chen, D. Isard, and B. Chance, 1986: A variational assimilation method for satellite and conventional data: Development of basic model for diagnosis of cyclone systems. NASA Con. Report. 3981, 223 pp.

Anthes, R. A., and T. T. Warner, 1978: Development of hydrodynamic models suitable for air pollution and other mesometeorological studies. Mon. Wea. Rev., 106, 1045-1078.

Barnes, S. L., 1973: Mesoscale objective analysis using weighted time-series observations. NOAA Tech. Memo. ERL NSSL-62, National Severe Storms Laboratory, Norman, OK 73069, 60 pp. (NTIS COM-73-10781).

Barnes, S. L., 1964: A technique for maximizing details in numerical weather map analysis. J. Appl. Meteor., 3, 396-409.

Bjilsma, S. J., L. M. Hafkenscheid and P Lynch, 1986: Computation of the streamfunction and velocity potential and reconstruction of the wind field. Mon. Wea. Rev., 114, 1547-1551.

Bloom, S. C., 1983: The use of dynamical constraints in the analysis of mesoscale rawinsonde data. Tellus, 35, 363-378.

Chance, B. A., 1986: Application of satellite data to the variational analysis of the three dimensional wind field. NASA Con. Rept. 4022, 86 pp.

Charney, J. G., 1948: On the scale of atmospheric motion. Geofys. Publikas., 17, 1-17.

Courant, R., 1936: Differential and Integral Calculus, Vol. 2, (E. J. McShane, translator), Wiley - Interscience, p198.

Dickerson, M. H., 1978: MASCON - A mass consistent atmospheric flux model for regions with complex terrain. J. Appl. Meteor., 17, 241-253.

Endlich, R. M., 1967: An iterative method for altering the kinematic properties of wind fields. J. Meteor., 6, 837-844.

Fjortoft, R., 1952: On a numerical method of integrating the barotropic vorticity equation. Tellus, 4, 179-194.

Fuelberg, H. E., 1974: Reduction and error analysis of the AVE II pilot experiment data. NASA CR-120496, Marshall Space Flight Center, Alabama, p. 60.

Gary, J. M., 1973: Estimate of truncation error in transformed coordinate primitive equation atmospheric models. J. Atmos. Sci., 30, 223-233.

Haltiner, G. J., 1971: Numerical Weather Prediction, Wiley and Sons, USA, 46-61.

Hawkins, H. F., and S. L. Rosenthal, 1965: On the computation of stream functions from the wind field. Mon. Wea. Rev., 93, 245-253.

Hovermale, J. B., 1962: A comparison of data accuracy in the troposphere and in the stratosphere. Dept. Meteorology, Penn. State Univ., Contract AF 19-(604)-6261, Rept. No. 2.

Janjic, Z. I., 1977: Pressure gradient force and advection scheme used for forecasting with steep and small scale terrain. Beitr. Phys. Atmos., 50, 186-199.

Janjic, Z. I., 1989: On the pressure gradient force error in σ-coordinate spectral models. Mon. Wea. Rev., 117, 2285-2292.

Kurihara, Y., 1968: Note on finite difference expressions for the hydrostatic relation and pressure gradient force. Mon. Wea. Rev., 96, 654-656.

Lewis, J. M., 1982: Adaptation of P.D. Thompson's scheme to the constraint of potential vorticity conservation. Mon. Wea. Rev., 110, 1618-1634.

Lewis, J. M., 1980: Dynamical adjustment of 500 mb vorticity using P.D. Thompson's scheme - a case study. Tellus, 32, 511-514.

Lewis, J. M., 1972: The operational upper air analysis using the variational method. Tellus, 24, 514-530.

Lewis, J. M., and T.H. Grayson, 1972: The adjustment of surface wind and pressure by Sasaki's variational matching technique. J. Appl. Meteor., 11, 586-597.

Lewis, J. M., C. M. Hayden and A. J. Schreiner, 1983: Adjustment of VAS and RAOB geopotential analysis using quasi-geostrophic constraints. Mon. Wea. Rev., 111, 2058-2067.

Lewis, J. M., and J. C. Derber, 1985: The use of adjoint equations to solve a variational adjustment problem with advective constraints. Tellus, 37A, 309-322.

Lynch, P., 1988: Deducing the wind from vorticity and divergence. Mon. Wea. Rev., 116, 86-93.

Mesinger, G., and A. Arakawa, 1976: Numerical methods used in atmospheric models. Vol. 1, GARP Publications Series No. 17, p47.

O'Brien, J.J., 1970: Alternative solutions to the classical vertical velocity problem. J. Appl. Meteor., 9, 197-203.

Ray, P. S., K. K. Wagner, K. W. Johnson, J. J. Stephens, W. C. Bumgarner, and E. A. Mueller, 1978: Triple-Doppler observations of a convective storm. J. Appl. Meteor., 17, 1201-1212.

Sangster, W. E., 1960: A method of representing the horizontal pressure force without reduction of pressures to sea level. J. Meteor., 17, 166-176.

Sasaki, Y., 1958: An objective analysis based upon the variational method. J. Meteor. Soc. Japan, 36, 77-88.

Sasaki, Y., 1970: Some basic formalisms in numerical variational analysis. Mon. Wea. Rev., 98, 875-883.

Schaefer, J. T., and C. A. Doswell III, 1979: On the interpolation of a vector field. Mon. Wea. Rev., 107, 458-476.

Sherman, C. A., 1978: A mass consistent model for wind fields over complex terrain. J. Appl. Meteor., 17, 312-319.

Shuman, F., and J. B. Hovermale, 1968: An operational six-layer primitive equation model. J. Appl. Meteor., 7, 525-547.

Shukla, J., and K. R. Saha, 1974: Computation of non-divergent stream function and irrotational velocity potential from the observed winds. Mon. Wea. Rev., 102, 419-425.

Sundqvist, H., 1975: On truncation errors in sigma-system models. Atmosphere, 13, 81-95.

Sundqvist, H., 1976: On vertical interpolation and truncation in conexion with use of sigma system models. Atmosphere, 14, 37-52.

Whittaker, E., and G. Robinson, 1926: The Calculus of Observations, (2nd Edition). London, Blackie and Son, Ltd., p.176.

Table 1

Nondimensional standard errors of observation for wind, height, and temperature and RMS errors for other adjustable meteorological variables.

Model Level	Pressure (mb)	VARIABLE u_{20}	u_{40}	Φ	$\Delta\Phi/\Delta x$	$\Delta\Phi/\Delta\sigma$	Mean Temp	σ	ϵ_u
								0.00	
10	100	0.45	0.23	0.25	0.71				
							3.68	0.59	2.13	6.98
9	200	0.45	0.23	0.20	0.56				
							3.21	0.88	1.88	6.98
8	300	0.42	0.21	0.18	0.51				
							2.28	0.88	1.64	6.51
7	400	0.36	0.18	0.15	0.42				
							1.53	0.76	1.43	5.58
6	500	0.32	0.16	0.12	0.33				
							0.97	0.59	1.24	4.65
5	600	0.30	0.15	0.09	0.26				
							0.61	0.44	1.04	4.34
4	700	0.28	0.14	0.08	0.22				
							0.53	0.44	0.84	3.72
3	800	0.24	0.12	0.07	0.20				
							0.47	0.44	0.64	3.26
2	900	0.21	0.11	0.06	0.18				
							0.42	0.44	0.44	3.10
1	1000	0.20	0.10	0.06	0.17				

Table 2

Nondimensional precision modulus weights for variational objective analysis.

Model Level	Pressure (mb)	VARIABLE u_{20}	Φ	$\Delta\Phi/\Delta x$	$\Delta\Phi/\Delta\sigma$	Mean Temp	σ	ϵ_u
							100	
10	100	2.5	8.0	1.0				
					0.04	1.4	10	0.01
9	200	2.5	12.5	1.6				
					0.05	0.6	0.14	0.01
8	300	2.8	15.4	1.9				
					0.10	0.6	0.19	0.01
7	400	3.9	22.2	2.8				
					0.21	0.9	0.24	0.02
6	500	4.9	34.7	4.6				
					0.53	1.4	0.33	0.02
5	600	5.6	61.7	7.4				
					1.34	2.6	0.46	0.03
4	700	6.4	78.1	10.3				
					1.78	2.6	0.71	0.04
3	800	8.7	102.0	12.5				
					2.26	2.6	1.22	0.05
2	900	11.3	138.9	15.4				
					2.83	2.6	2.58	0.05
1	1000	12.5	138.9	17.3				

Table 3. Correlation coefficients for a 216-point subset of initial (i) and variational (v) u, v, and T 3-h forward tendencies at 0000 UTC compared with observed 3-h tendencies centered at 0130 UTC.

p lev	u_i	u_v	v_i	v_v	T_i	T_v
200	-0.34	-0.08	-0.27	-0.25	0.17	0.07
300	-0.10	-0.24	0.43	0.10	-0.36	0.17
400	-0.24	0.12	0.53	0.35	0.24	0.59
500	-0.26	0.31	0.43	0.71	0.75	0.65
600	0.36	0.56	0.01	0.35	0.42	0.75
700	0.66	0.71	0.15	0.61	0.55	0.72
800	0.55	0.59	0.54	0.79	0.48	0.17
900	0.65	0.60	0.31	0.37	0.25	0.22

Table 4. Same as Table 1 but with 0000 UTC 3-h forward tendencies shifted by weather system translation to approximate 0130 UTC observed tendencies.

p lev	u_i	u_v	v_i	v_v	T_i	T_v
200	-0.35	-0.06	-0.31	-0.25	0.12	0.02
300	0.01	-0.04	0.56	0.23	-0.31	0.14
400	-0.27	0.20	0.45	0.30	0.35	0.67
500	-0.03	0.57	0.54	0.73	0.83	0.64
600	0.56	0.69	0.02	0.45	0.57	0.76
700	0.79	0.83	0.22	0.73	0.66	0.71
800	0.72	0.75	0.60	0.87	0.55	0.23
900	0.82	0.78	0.35	0.48	0.32	0.49

FIGURE CAPTIONS

Fig. 1. The distribution of rawinsonde stations over the analysis grid (solid rectangle), evaluation grid (large dashed rectangle), and SESAME I network (small dashed rectangle).

Fig. 2. Residual reduction as a function of cycle for the u-component (left panel) and v-component (right panel) dynamic constraints.

Fig. 3. Residual reduction as a function of cycle for the integrated continuity equation (left panel), the hydrostatic equation (middle panel), and the thermodynamic equation (right panel).

Fig. 4. RMS differences between unadjusted (adjusted) fields and observations after removal of standard observation error (solid lines) and means of differences between unadjusted (adjusted) fields and observations (dashed lines) for a) heights, b) temperatures, c) u-comp, and d) v-comp.

Fig. 5. Heights and wind vectors at 800 mb, 500 mb, and 300 mb for a) unadjusted and b) adjusted fields.

Fig. 6. Differences between adjusted and unadjusted heights and vector winds at 800 mb, 500 mb, and 300 mb.

Fig. 7. Same as Fig. 5 but for temperature.

Fig. 8. Relative vorticities at 500 mb, a) unadjusted and b) adjusted.

Fig. 9. a) unadjusted, b) adjusted vertical velocities (cm sec^{-1}) at 500 mb. Precipitation areas are stippled.

Fig. 10. u-component tendencies for 800 mb (left panels) and 500 mb (right panels) for a) observed, b) unadjusted, and c) adjusted fields in m sec^{-1} 3-hr^{-1}.

Fig. 11. Same as Fig. 10 but for the v-component.

Fig. 12. u-component tendencies (left panels) and v-component tendencies (right panels) at 300 mb for a) observed, b) unadjusted, and c) adjusted fields in m sec^{-1} 3-hr^{-1}.

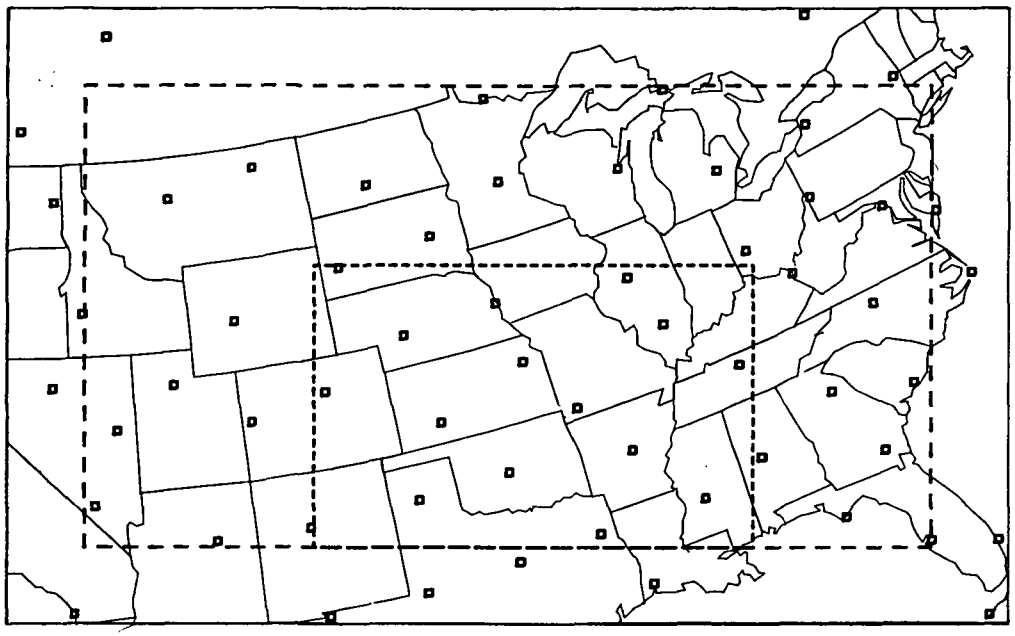

Fig. 1. The distribution of rawinsonde stations over the analysis grid (solid rectangle), evaluation grid (large dashed rectangle), and SESAME I network (small dashed rectangle).

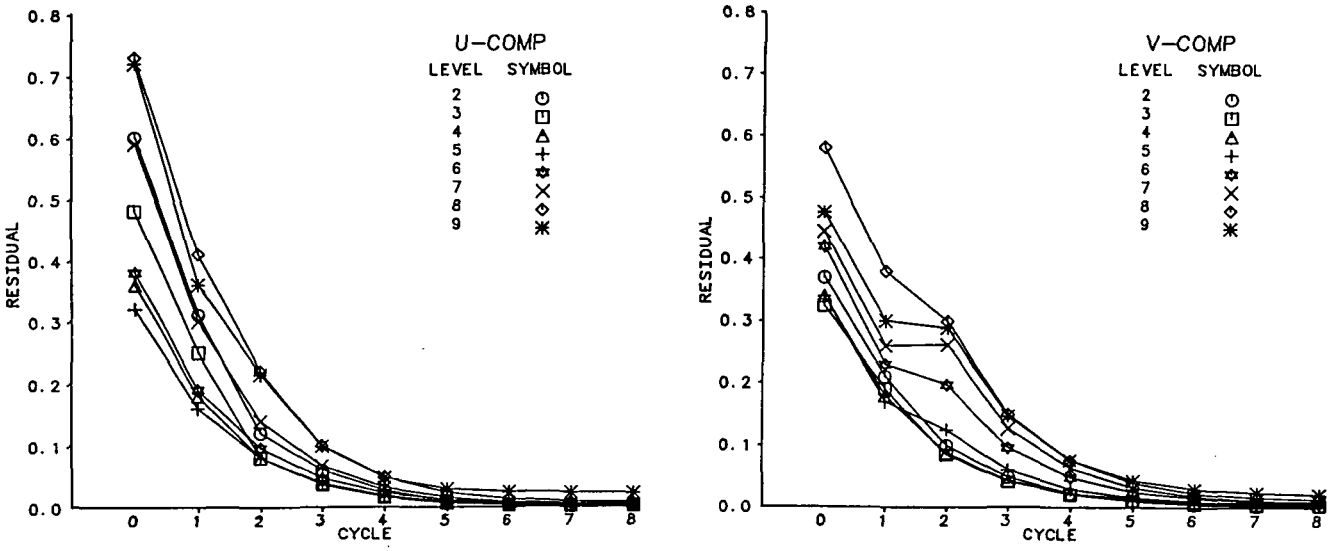

Fig. 2. Residual reduction as a function of cycle for the u-component (left panel) and v-component (right panel) dynamic constraints.

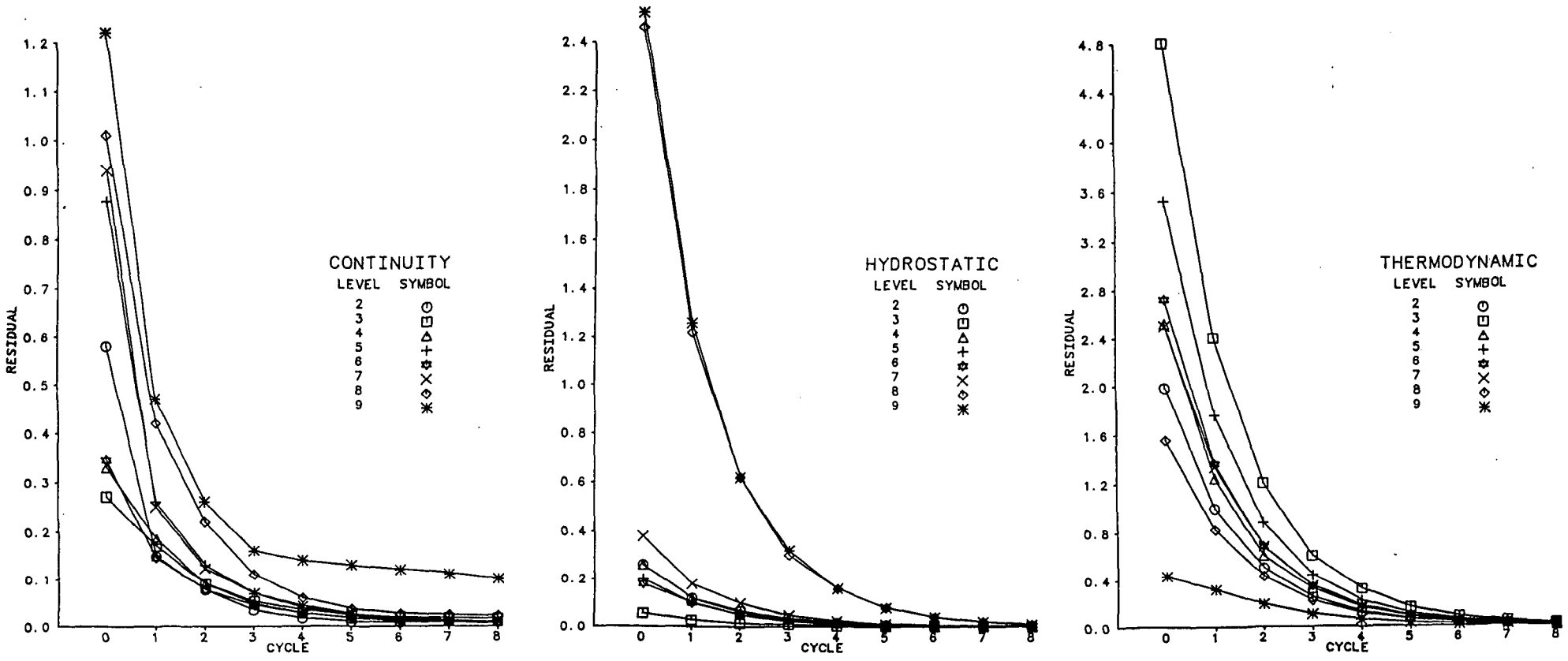

Fig. 3. Residual reduction as a function of cycle for the integrated continuity equation (left panel), the hydrostatic equation (middle panel), and the thermodynamic equation (right panel).

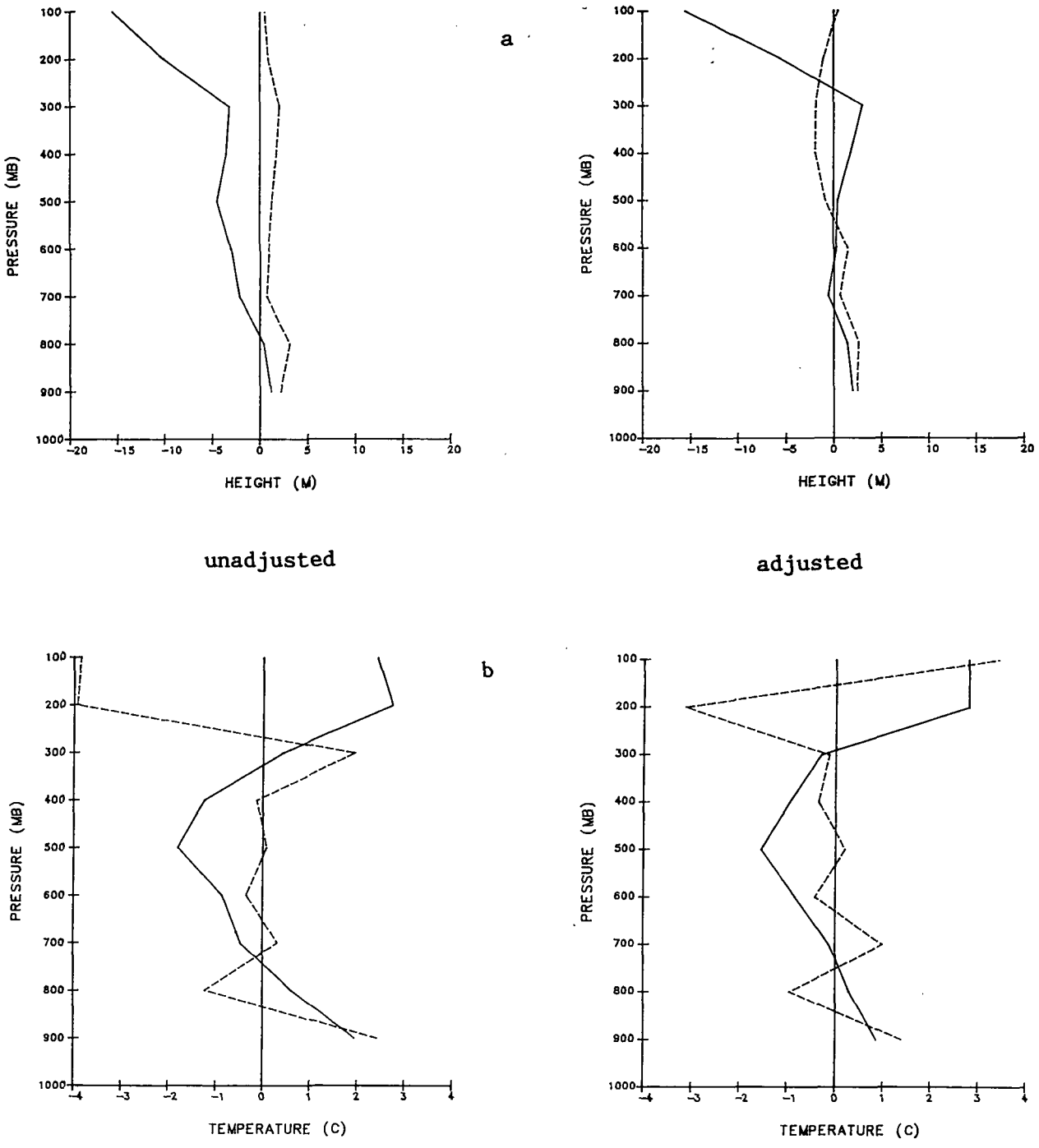

Fig. 4. RMS differences between unadjusted (adjusted) fields and observations after removal of standard observation error (solid lines) and means of differences between unadjusted (adjusted) fields and observations (dashed lines) for a) heights, b) temperatures, c) u-comp, and d) v-comp.

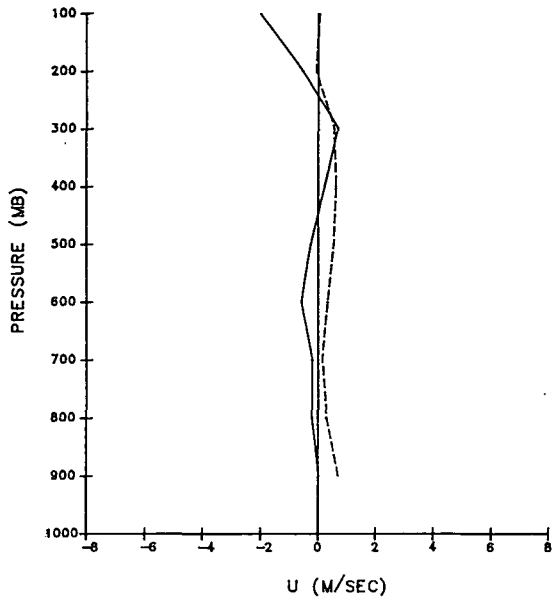

unadjusted

c

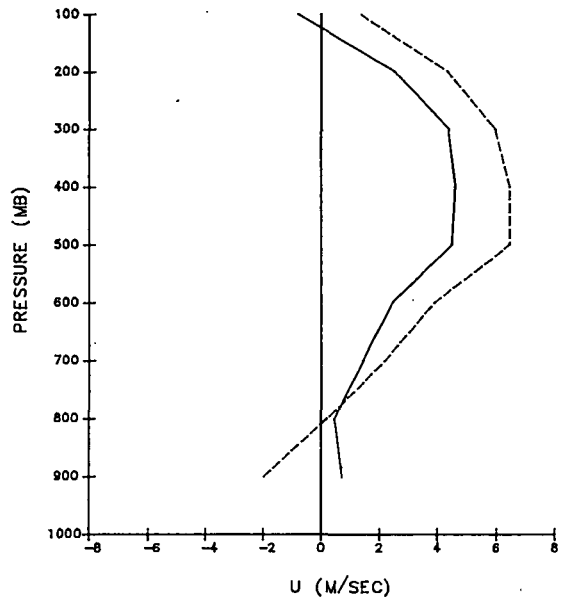

adjusted

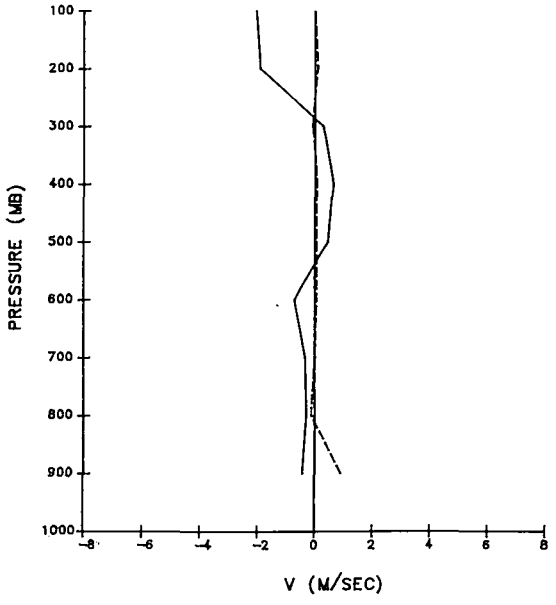

d

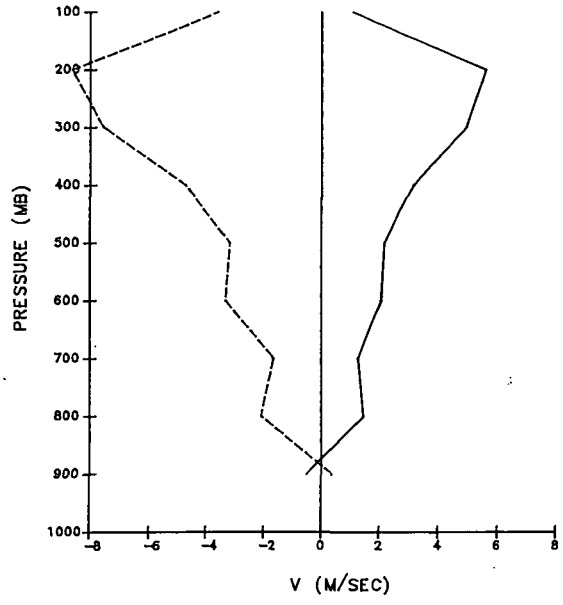

a b

300 mb

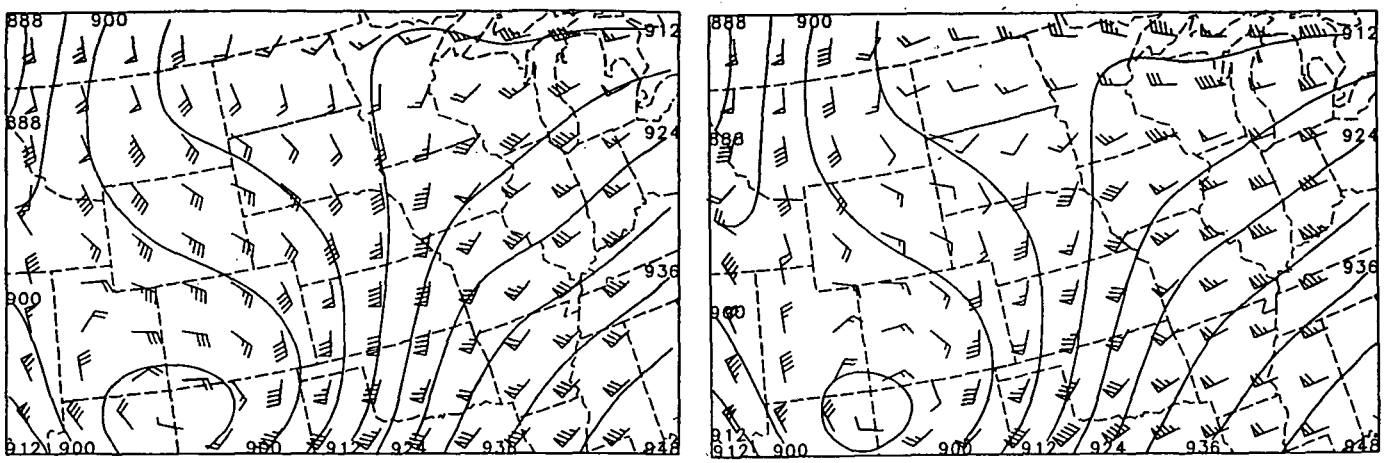

500 mb

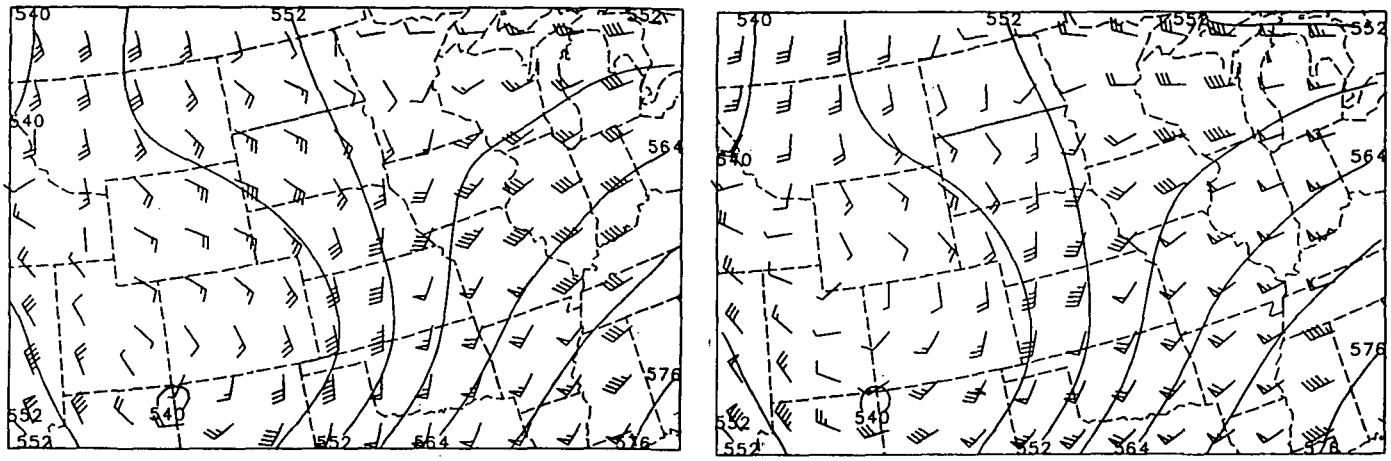

800 mb

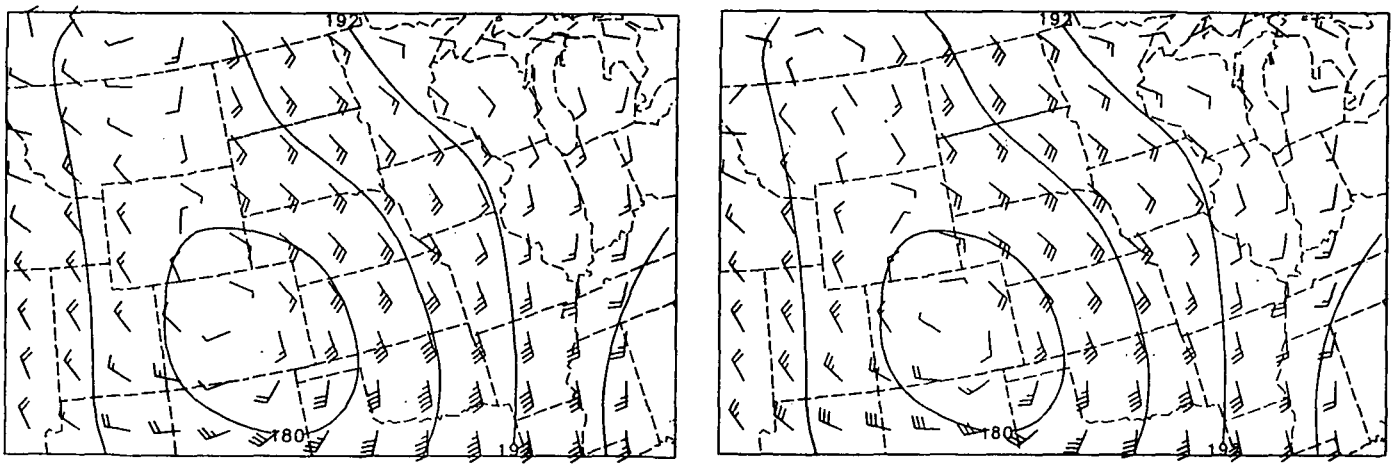

Fig. 5. Heights and wind vectors at 800 mb, 500 mb, and 300 mb for a) unadjusted and b) adjusted fields.

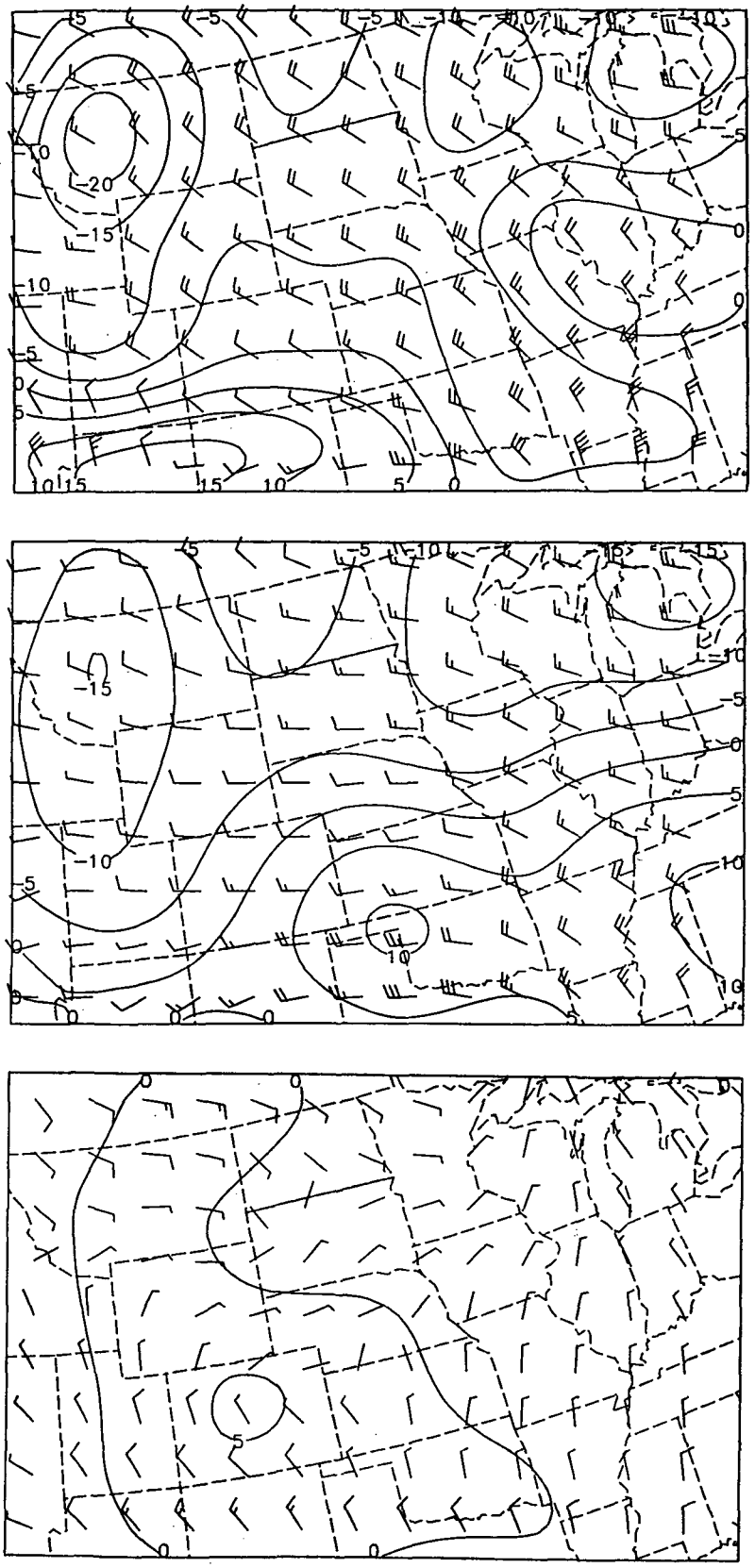

Fig. 6. Differences between adjusted and unadjusted heights and vector winds at 800 mb, 500 mb, and 300 mb.

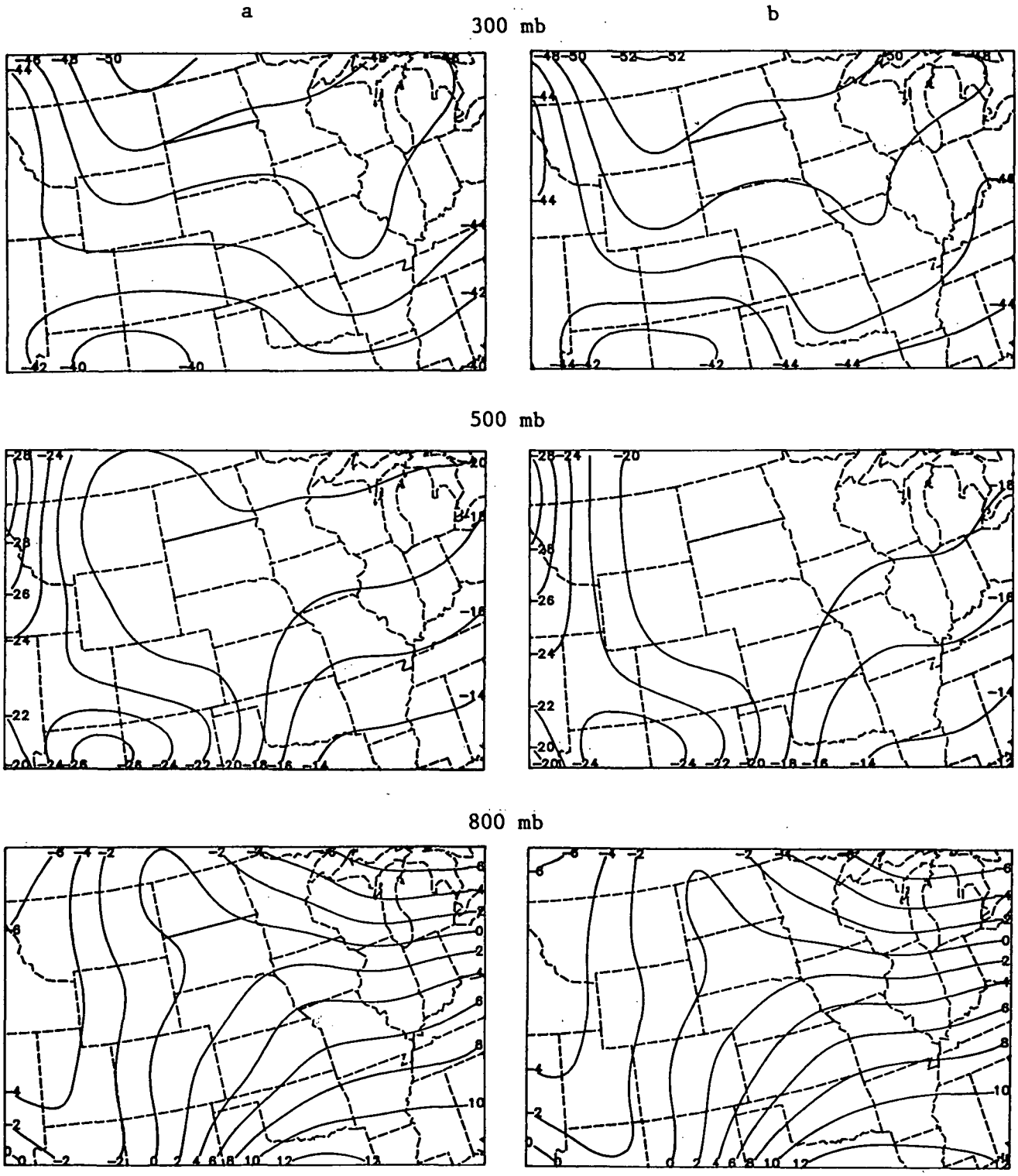

Fig. 7. Same as Fig. 5 but for temperature.

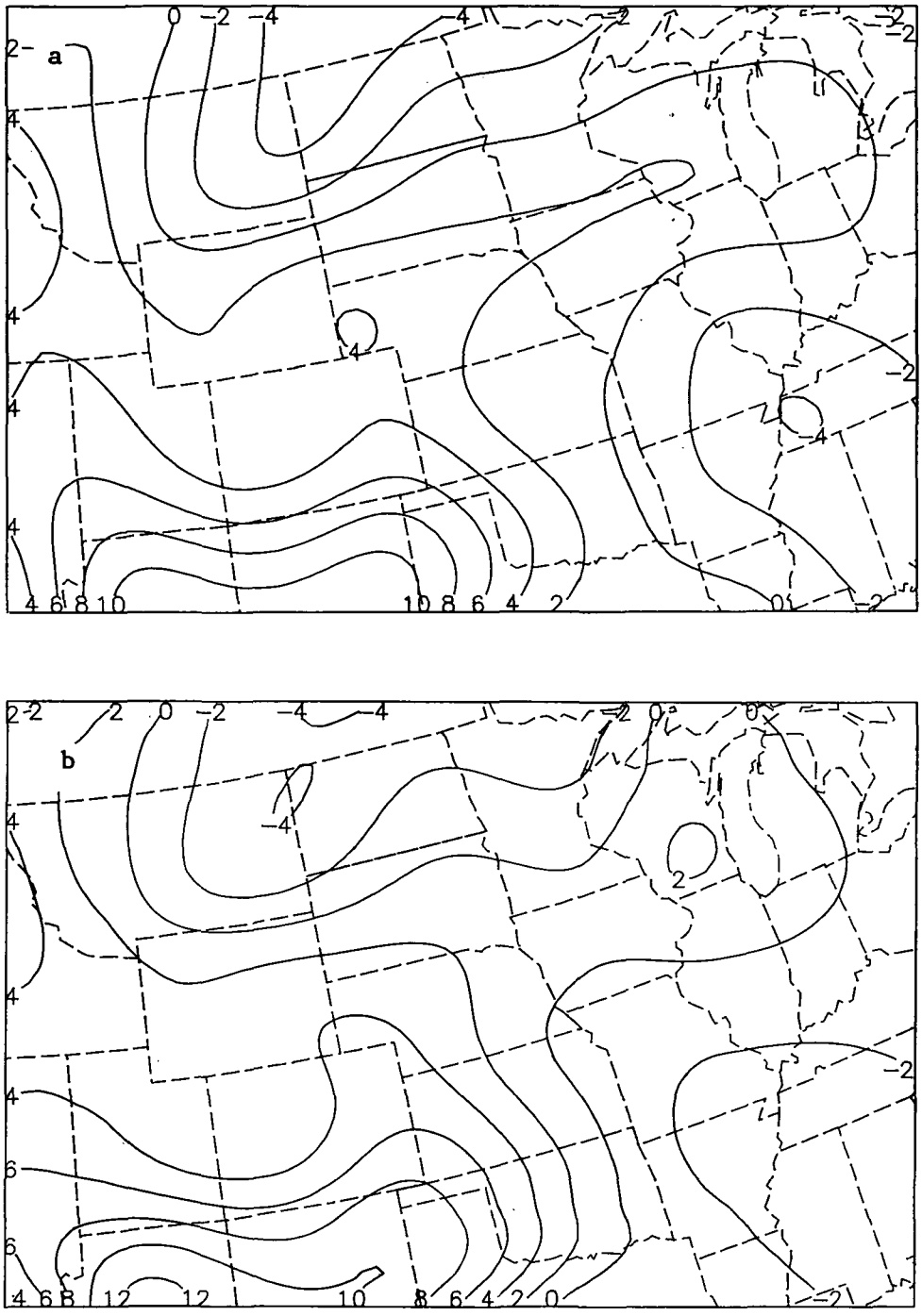

Fig. 8. Relative vorticities at 500 mb, a) unadjusted and b) adjusted.

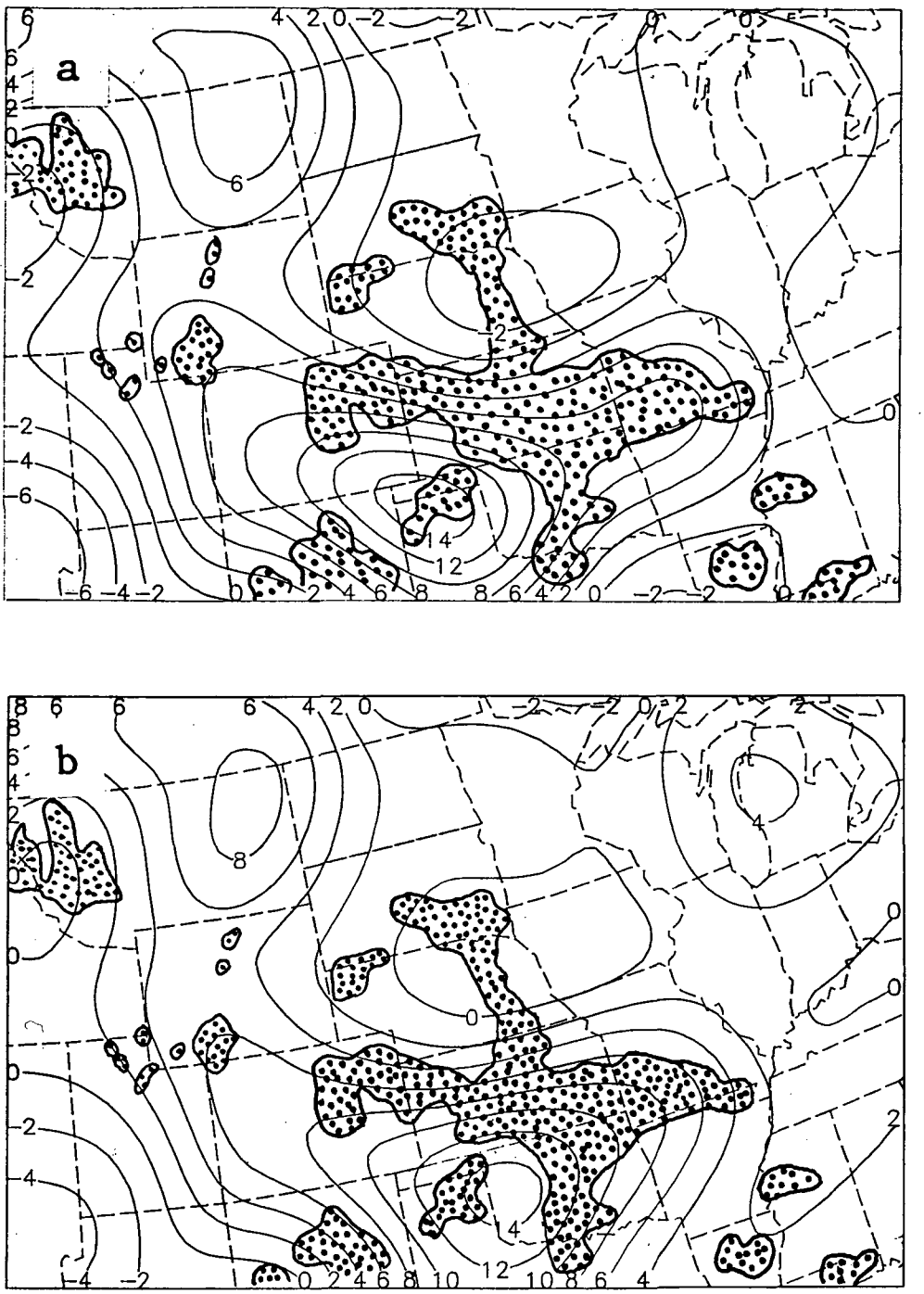

Fig. 9. a) unadjusted, b) adjusted vertical velocities (cm sec^{-1}) at 500 mb. Precipitation areas are stippled.

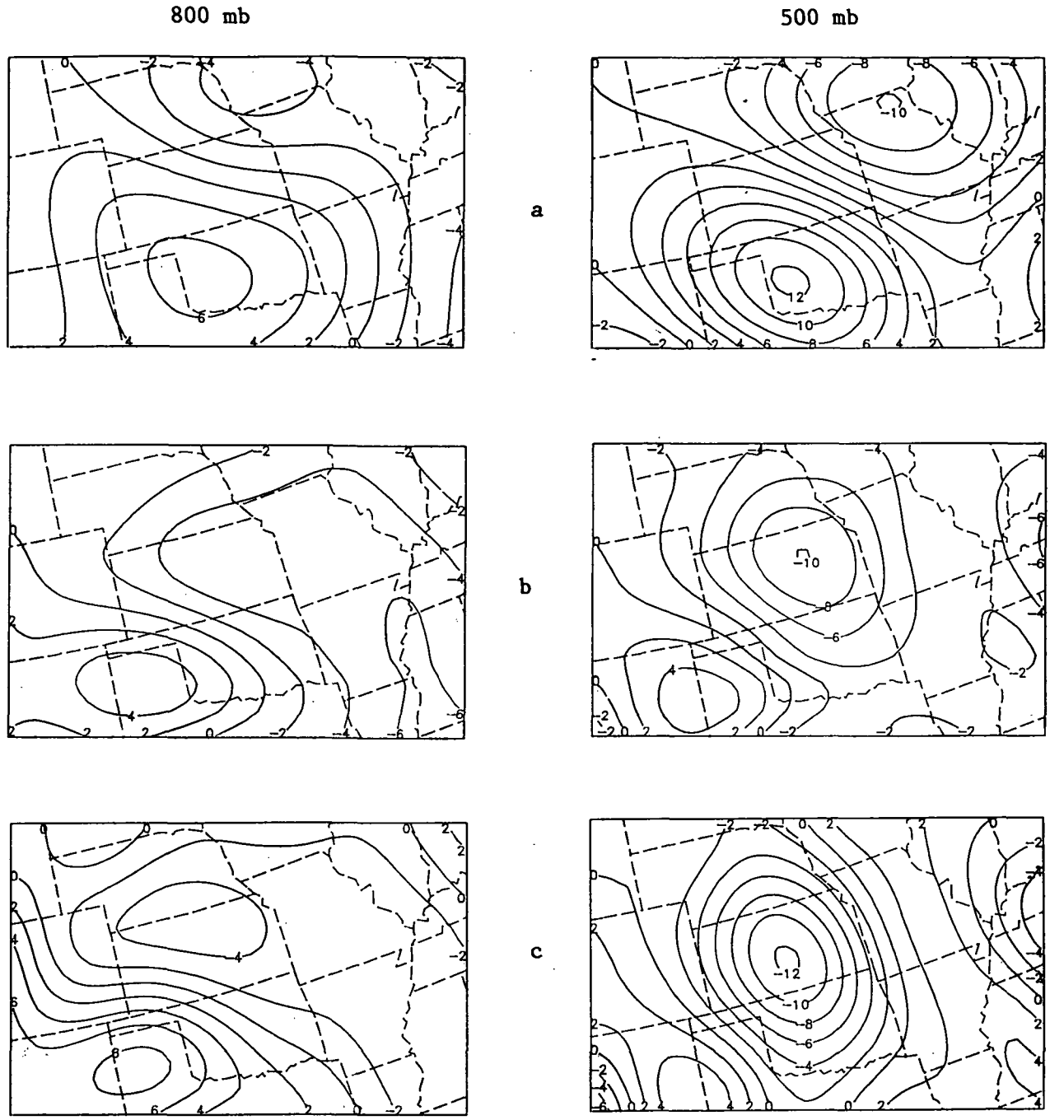

Fig. 10. u-component tendencies for 800 mb (left panels) and 500 mb (right panels) for a) observed, b) unadjusted, and c) adjusted fields in m sec^{-1} 3-hr^{-1}.

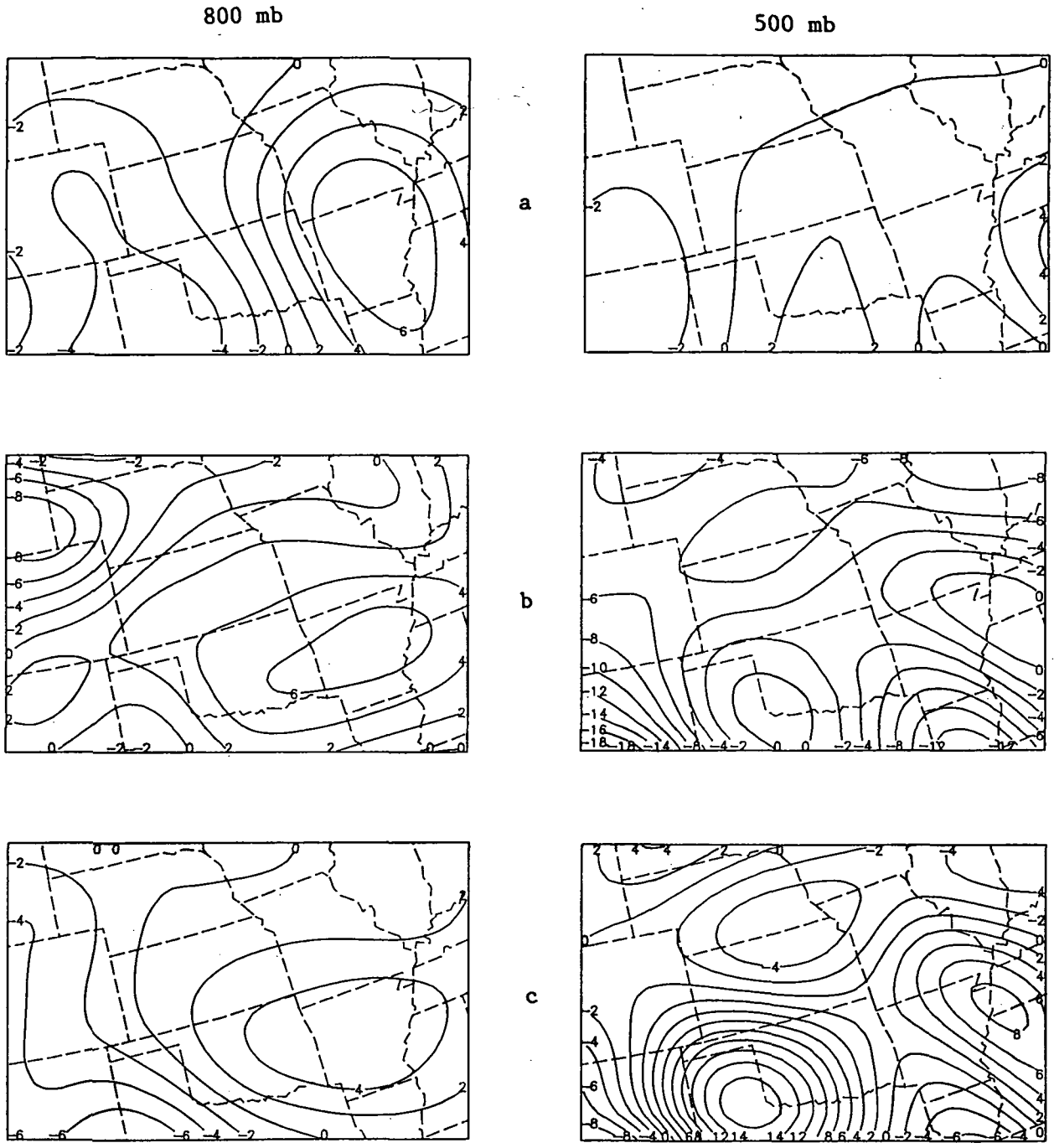

Fig. 11. Same as Fig. 10 but for the v-component.

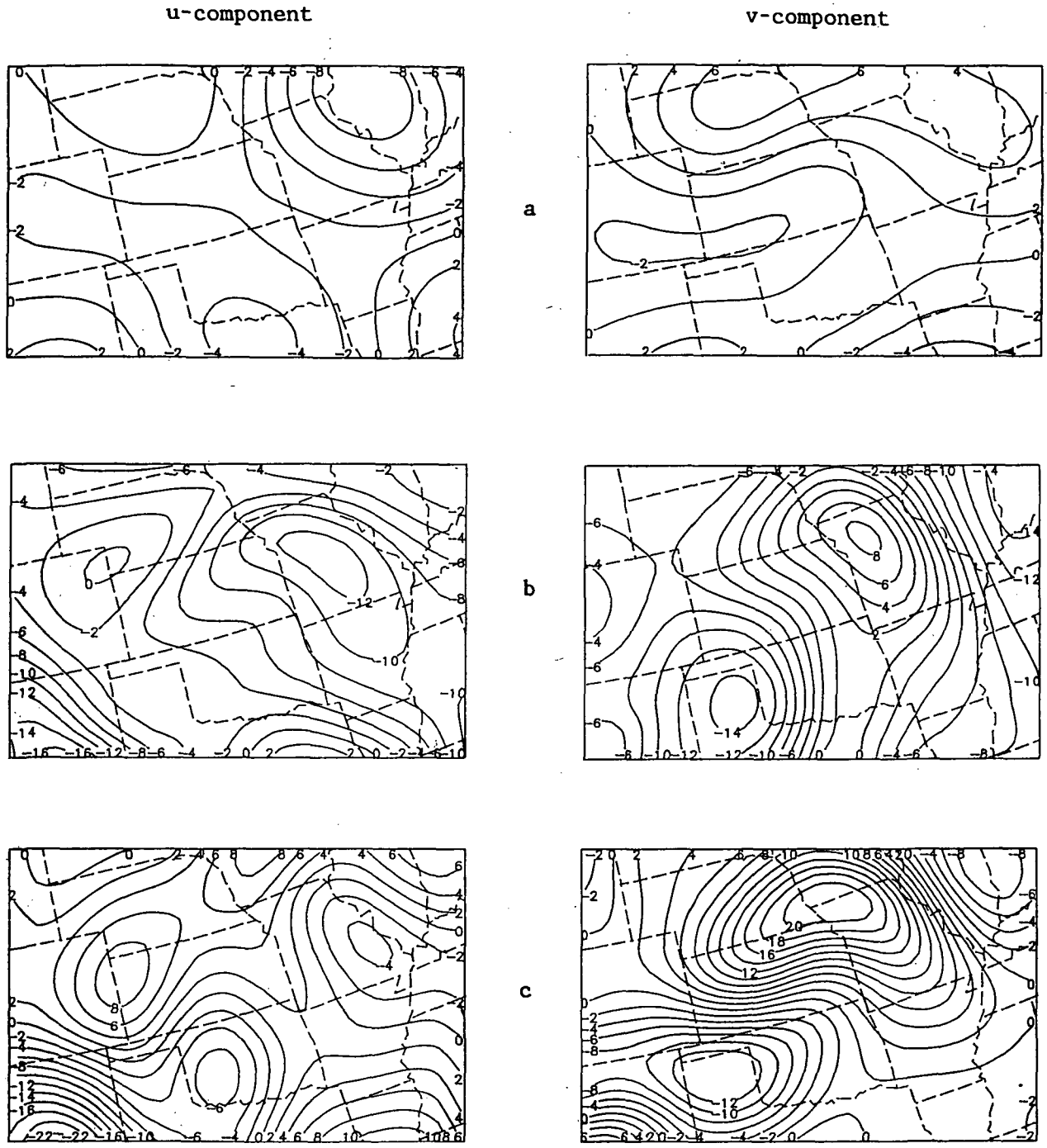

Fig. 12. u-component tendencies (left panels) and v-component tendencies (right panels) at 300 mb for a) observed, b) unadjusted, and c) adjusted fields in m sec^{-1} 3-hr^{-1}.